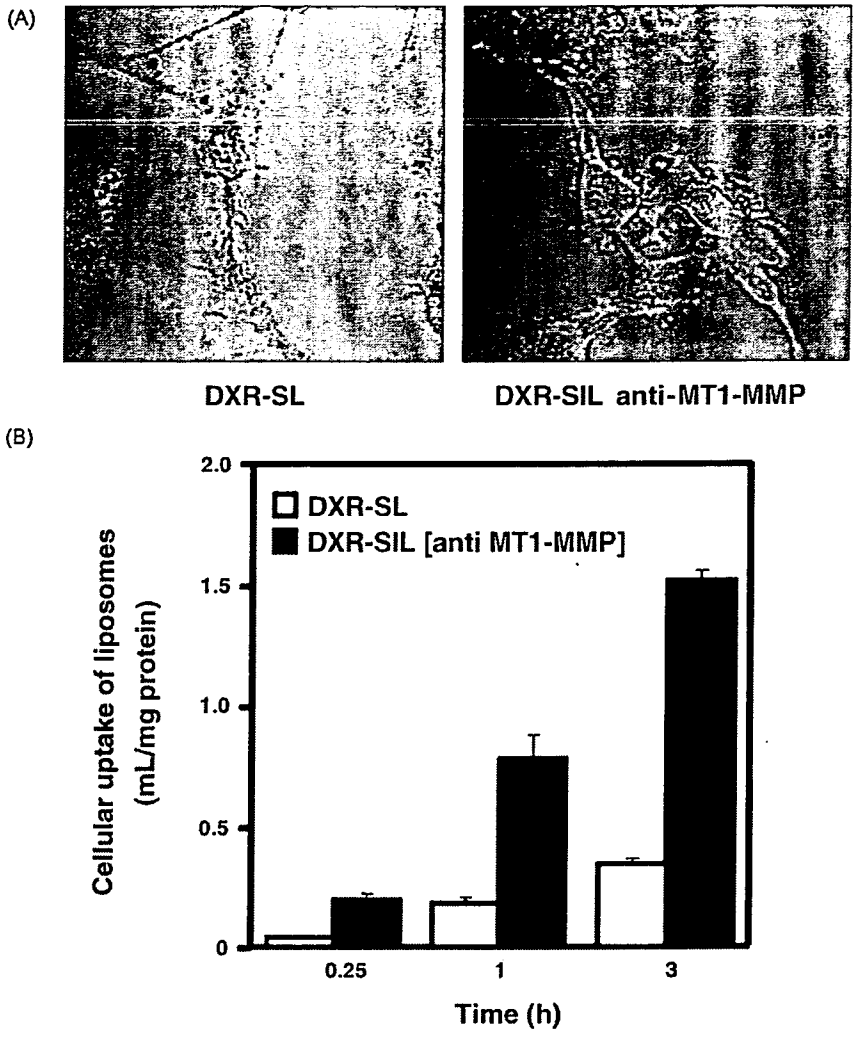

Fig. 1. Cellular uptake of DXR-SIL[anti-MT1-MMP(Fab')] and DXR-SL to the HT1080 cells. (A) DXR-SIL[anti-MT1-MMP(Fab')] (right panel) and DXR-SL (left panel) were incubated with HT1080 cells for 3 h. Cells were washed, and then intracellular accumulation of encapsulated doxorubicin was fluorescently visualized with CLSM. (B) [^{14}C]-DXR-SIL[anti-MT1-MMP(Fab')] (closed bars) and DXR-SL (opened bars) were incubated with HT1080 cells. At indicated time, cells were washed and then cellular radioactivity was counted by liquid scintillation counter. Cellular radioactivity was normalized by the protein amount of the sample. Data were represented as mean ± S.D. ($n = 3$).

($n = 6$), respectively. Fig. 2 showed the time profiles for the relative tumor volume up to 12 days after administration of liposomal formulations. When DXR-SL was administered, tumor volume was decreased in only 1 out of 6 mice at 12 days (Fig. 2A). Furthermore, three of six mice died up to 12 day, the body weights of which were drastically decreased (14.8%, 17.7%, and 17.8%, respectively), presumably by the side effect of DXR-SL. In contrast, in the case of DXR-SIL[anti-MT1-

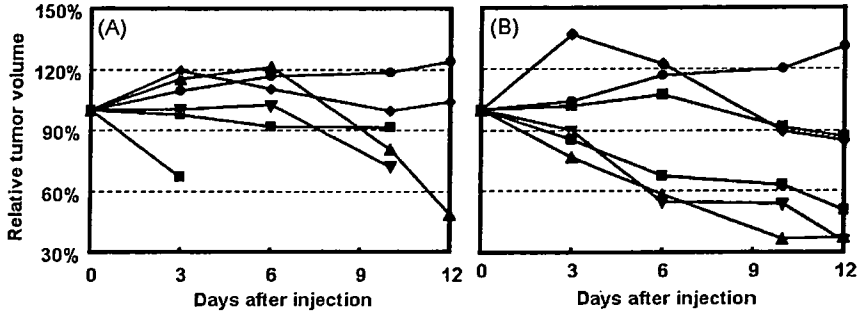

Fig. 2. Time profiles of the tumor volume after the single i.v. injection of DXR-SIL[anti-MT1-MMP(Fab')] and DXR-SL. DXR-SIL[anti-MT1-MMP(Fab')] and DXR-SL were injected from tail vein at a dose of 3 mg/kg DXR and 5 μmol lipid/mouse. Tumor volume was measured just before the injection, and up to 12 days after the injection. The data of six individual mice were plotted. (A) and (B) represented the data after the injection of DXR-SL and DXR-SIL[anti-MT1-MMP(Fab')], respectively.

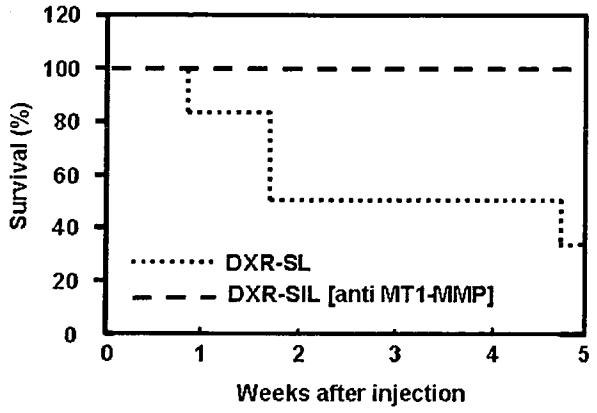

Fig. 3. Time profiles for the survival rate of mice after the single injection of DXR-SIL[anti-MT1-MMP(Fab′)] and DXR-SL. After the single i.v. administration of DXR-SIL[anti-MT1-MMP(Fab′)] and DXR-SL, survival of six mice was followed up until 5 weeks.

MMP(Fab′)], tumor volume decreased efficiently in half of mice at 12 days (Fig. 2B). Furthermore, whereas one mouse showed notably body weight change (20.1%), no mouse died. These results suggested that DXR-SIL[anti-MT1-MMP(Fab′)] would be superior to that of DXR-SL from the point of view of antitumor activity and less side effect. As shown in Fig. 3, administration of DXR-SIL [anti-MT1-MMP] exhibited prolonged survival compared with that of DXR-SL, presumably because of the temporal inhibition of tumor growth after the administration. These data suggested that DXR-SIL [anti-MT1-MMP] was more potent in the pharmacological activity than that of DXR-SL.

3.4. Comparison of in vivo tumor distribution

The amino acid sequence of human MT1-MMP is highly homologous approximately 96% matching with mouse MT1-MMP. Therefore, it is plausible that 222-1D8 cross-react with mouse MT1-MMP. Considering that MT1-MMP was expressed on the neovascular membrane, more potent antitumor activity can be attributed to the efficient accumulation of the liposomes via the targeting function of the Fab′ fragment. To measure the distribution of DXR in the tumor, [^{14}C]-DXR-SIL[anti-MT1-MMP(Fab′)] and [^{14}C]-DXR-SL were administered intravenously, and then radioactivities in blood sample and tumor were measured after 48 h. As a result, blood concentration of DXR encapsulated in SIL[anti-MT1-MMP(Fab′)] and in SL was comparable, indicating that modification of $Fab'_{222\text{-}1DB}$ did not alter the tumor accumulation of these liposomes (Fig. 4A). This is inconsistent with a previous observation in OX-26-modified PEG liposomes (Huwyler et al., 1996), which is designed as the targeting vector for transferrin receptor (TfR)-expressing organs. In that study, OX-26-modified immunosterically stabilized liposomes were rapidly eliminated from the blood circulation compared with non-targeted sterically stabilized liposomes, when more than 20 of OX-26 antibodies were conjugated. In contrast, in the present study, retention of DXR-SIL[anti-MT1-MMP(Fab′)] in the blood circulation was comparable even though the DXR-SIL[anti-MT1-MMP(Fab′)] were expected to have approximately 40 of $Fab'_{222\text{-}1DB}$. The antibody-dependent difference in the blood concentration of liposomes may be accounted for by the tissue distribution of transferrin receptor and MT1-MMP. Since transferrin receptors were ubiquitously and widely expressed at various organs (Hatakeyama et al., 2004; Ponkaand and Lok, 1999; Qian et al., 2002), systemic OX-26-modified immunoliposomes may be cleared by various organs, in addition to the RES. In contrast, the expression of MMPs remained few at normal condition and induced only at the pathological condition such as inflammation and malignant alternation (Sato et al., 1994; Pagenstecher et al., 1998). It is likely that clearance of the $Fab'_{222\text{-}1DB}$-modified immune-sterically stabilized liposomes (SIL[anti-MT1-MMP(Fab′)]) was mainly governed by RES as is the case of non-targeted liposomes (SL).

Then, tumor accumulation of DXR-SIL[anti-MT1-MMP(Fab′)] was compared with DXR-SL at 48 h after intravenous administration. Unexpectedly, the accumulation of DXR-SIL[anti-MT1-MMP(Fab′)] was comparable or slightly lower than that of DXR-SL, although MT1-MMP should be expressed in the neovascular membrane. This result is

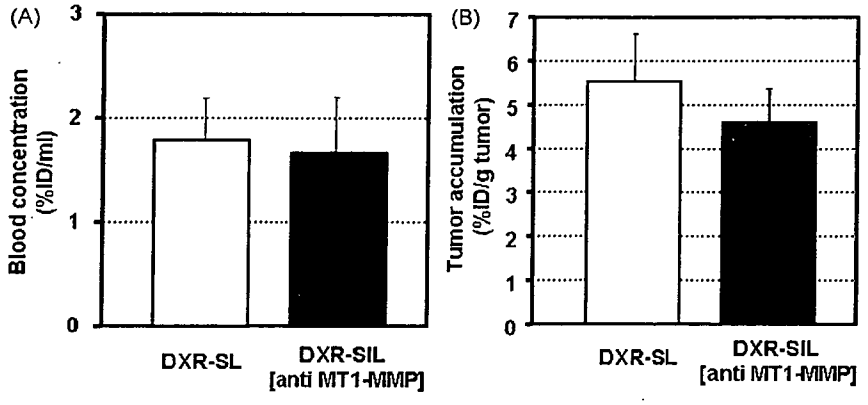

Fig. 4. Blood concentration and tumor accumulation of [^{14}C]-DXR-SIL[anti-MT1-MMP(Fab′)] and [^{14}C]-DXR-SL. At 48 h post-injection of [^{14}C]-DXR-SIL[anti-MT1-MMP(Fab′)] and DXR-SL at a dose of 0.15 μmol lipids/mouse, the mice was sacrificed and blood and tumor were collected. Radioactivities in the blood and tumor tissue were determined by liquid scintillation counter. The data of blood concentration and tumor accumulation of DXR are shown in (A) and (B), respectively. Data are represented by mean ± S.D. ($n = 3$).

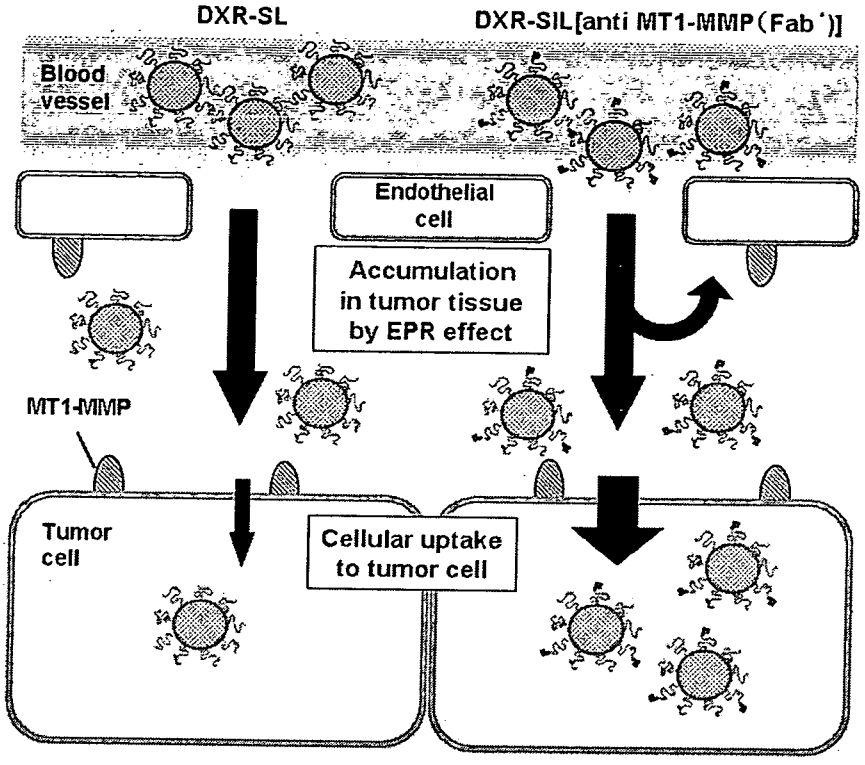

Fig. 5. Schematic diagram illustrating a possible mechanism for the tumor cell and/or neovascular cells by means of DXR-SIL[anti-MT1-MMP(Fab')]. Since tumor accumulation of DXR-SIL[anti-MT1-MMP(Fab')] was comparable to DXR-SL, DXR-SIL[anti-MT1-MMP(Fab')] may accumulate in tumor mainly via EPR effect as is the case of DXR-SL. After they accumulate in the tissue, DXR-SIL[anti-MT1-MMP(Fab')] efficiently internalize by virtue of a function of $Fab'_{222\text{-}1D8}$ modified on the distal end of PEG.

inconsistent with the previous observation that liposomes modified with peptides having binding activity to MT1-MMP showed highly tumor accumulation compared with non-targeting liposomal formulation (Kondo et al., 2004). It can be accounted for by assuming the difference of the investigation time after administration. In the previous peptide-modified liposomes, accumulation was evaluated just after injection. Then, contribution of EPR effect on tumor accumulation would be minor. However, in the present study, the tumor distribution was measured at 48 h after i.v. administration. Therefore, the liposomal accumulation in tumor may be mainly achieved by EPR effect, rather than active targeting via the specific antibody. Furthermore, considering the physiological role of MT1-MMP to digest the matrix, there is also the possibility that MT1-MMP was mainly expressed on the abluminal side but not on the apical side, and then both of DXR-SIL[anti-MT1-MMP(Fab')] and DXR-SL accumulated to the tumor mainly via EPR effect. Once accumulated in the tumor tissue, $Fab'_{222\text{-}1DB}$ function as an accelerator for the cellular uptake of SIL[anti-MT1-MMP(Fab')] by the neovascularity and tumor cells. In this sense, the Fab' fragment contributed to controlling intra-tumor disposition of liposomes, but not to the tissue targeting in systemic circulation (Fig. 5).

4. Conclusion

Fab' fragment ($Fab'_{222\text{-}1D8}$) against MT1-MMP was potent ligand, which may accelerate the cellular accumulation of doxorubicin-encapsulating sterically stabilized liposomes to the cancer cells and/or neovascular cells after they reached to the tumor tissue via EPR effect.

Acknowledgements

This work was supported in part by Grants-in-Aid for Scientific Research (B) and Grant-in-Aid for Young Scientists (B) from the Ministry of Education, Culture, Sports, Science and Technology of Japan, and by Grants-in-Aid for Scientific Research on Priority Areas from the Japan Society for the Promotion of Science.

References

Aoki, T., Yonezawa, K., Ohuchi, E., Fujimoto, N., Iwata, K., Shimada, T., Okada, Y., Seiki, M., 2002. Two-step sandwich enzyme immunoassay using monoclonal antibodies for detection of soluble and membrane-associated human membrane type 1-matrix metalloproteinase. J. Immunoassay Immunochem. 23, 49–68.

Čeh, B., Winterhalter, M., Frederik, P.M., Vallner, J.J., Lasic, D.D., 1997. Stealth liposomes: from theory to product. Adv. Drug Del. Rev. 24, 165–177.

Haran, G., Cohen, R., Bar, L.K., Barenholz, Y., 1993. Transmembrane ammonium sulfate gradients in liposomes produce efficient and stable entrapment of amphipathic weak bases. Biochim. Biophys. Acta 1151, 201–215.

Hatakeyama, H., Akita, H., Maruyama, K., Suhara, T., Harashima, H., 2004. Factors governing the *in vivo* tissue uptake of transferrin-coupled polyethylene glycol liposomes *in vivo*. Int. J. Pharm. 281, 25–33.

Huwyler, J., Wu, D., Pardridge, W.M., 1996. Brain drug delivery of small molecules using immunoliposomes. Proc. Natl. Acad. Sci. U.S.A. 93, 14164–14169.

Itoh, Y., Seiki, M., 2004. MT1-MMP: an enzyme with multidimensional regulation. Trends Biochem. Sci. 29, 285–289.

Klibanov, A.L., Maruyama, K., Torchilin, V.P., Hunag, L., 1990. Amphipathic polyethylenglycols effectively prolong the circulation time of liposomes. FEBS Lett. 268, 235–237.

Knauper, V., Will, H., Lopez-Otin, C., Smith, B., Atkinson, S.J., Stanton, H., Hembry, R.M., Murphy, G., 1996. Cellular mechanisms for human procollagenase-3 (MMP-13) activation. Evidence that MT1-MMP (MMP-14) and gelatinase a (MMP-2) are able to generate active enzyme. J. Biol. Chem. 271, 17124–17131.

Kondo, M., Asai, T., Sadzuka, Y., Katanasaka, Y., Ogino, K., Taki, T., Baba, K., Oku, N., 2004. Anti-neovascular therapy by liposomal drug targeted to membrane type-1 matrixmetalloproteinase. Int. J. Cancer 108, 301–306.

Lukyanov, A.N., Elbayoumi, T.A., Chakilam, A.R., Torchilin, V.P., 2004. Tumor-targeted liposomes: doxorubicin-loaded long-circulating liposomes modified with anti-cancer antibody. J. Control. Release 100, 135–144.

Maeda, N., Takeuchi, Y., Takada, M., Sadzuka, Y., Namba, Y., Oku, N., 2004. Anti-neovascular therapy by use of tumor neovasculature-targeted long-circulating liposomes. J. Control. Release 100, 41–52.

Maekawa, R., Maki, H., Yoshida, H., Hojo, K., Tanaka, H., Wada, T., Uchida, N., Takeda, Y., Kasai, H., Okamoto, H., Tsuzuki, H., Kambayashi, Y., Watanabe, F., Kawada, K., Toda, K., Ohtani, M., Sugita, K., Yoshioka, T., 1999. Correlation of antiangiogenic and antitumor efficacy of *N*-biphenyl sulfonyl-phenylalanine hydroxiamic acid (BPHA), an orally active, selective matrix metalloproteinase inhibitor. Cancer Res. 59, 1231–1235.

Maruyama, K., Takahashi, N., Tagawa, T., Nagaike, K., Iwatsuru, M., 1997. Immunoliposomes bearing polyethyleneglycol-coupled Fab′ fragment show prolonged circulation time and high extravasation into targeted solid tumors *in vivo*. FEBS Lett. 413, 177–180.

Matsumura, Y., Maeda, H., 1986. A new concept for macromolecular therapeutics in cancer chemotherapy: mechanism of tumoritropic accumulation of proteins and the antitumor agent smancs. Cancer Res. 46, 6387–6392.

Mendelsohnand, J., Baselga, J., 2003. Status of epidermal growth factor receptor antagonists in the biology and treatment of cancer. J. Clin. Oncol. 21, 2787–2799.

Nelson, N.J., 1998. Inhibitors of angiogenesis enter phase III testing. J. Natl. Cancer Inst. 90, 960–963.

Noel, A., Santavicca, M., Stoll, I., L'Hoir, C., Staub, A., Murphy, G., Rio, M.C., Basset, P., 1995. Identification of structural determinants controlling human and mouse stromelysin-3 proteolytic activities. J. Biol. Chem. 270, 22866–22872.

Ohuchi, E., Imai, K., Fujii, Y., Sato, H., Seiki, M., Okada, Y., 1997. Membrane type 1 matrix metalloproteinase digests interstitial collagens and other extracellular matrix macromolecules. J. Biol. Chem. 272, 2446–2451.

Pagenstecher, A., Stalder, A.K., Kincaid, C.L., Shapiro, S.D., Campbell, I.L., 1998. Differential expression of matrix metalloproteinase and tissue inhibitor of matrix metalloproteinase genes in the mouse central nervous system in normal and inflammatory states. Am. J. Pathol. 152, 729–741.

Pardridge, W.M., 2004. Intravenous, non-viral RNAi gene therapy of brain cancer. Expert Opin. Biol. Ther. 4, 1103–1113.

Pei, D., Weiss, S.J., 1996. Transmembrane-deletion mutants of the membrane-type matrix metalloproteinase-1 process progelatinase A and express intrinsic matrix-degrading activity. J. Biol. Chem. 271, 9135–9140.

Pei, D., Majmudar, G., Weiss, S.J., 1994. Hydrolytic inactivation of a breast carcinoma cell-derived serpin by human stromelysin-3. J. Biol. Chem. 269, 25849–25855.

Ponkaand, P., Lok, C.N., 1999. The transferrin receptor: role in health and disease. Int. J. Biochem. Cell Biol. 31, 1111–1137.

Qian, A.M., Li, H., Sun, H., ho, K., 2002. Targeted drug delivery via the transferrin receptor-mediated endocytosis pathway. Pharmacol. Rev. 54, 561–587.

Sato, H., Takino, T., Okada, Y., Cao, J., Shinagawa, A., Yamamoto, E., Seiki, M., 1994. A matrix metalloproteinase expressed on the surface of invasive tumour cells. Nature 370, 61–65.

Strongin, A.Y., Collier, I., Bannikov, G., Marmer, B.L., Grant, G.A., Goldberg, G.I., 1995. Mechanism of cell surface activation of 72-kDa type IV collagenase. Isolation of the activated form of the membrane metalloprotease. J. Biol. Chem. 270, 5331–5338.

Uekita, T., Itoh, Y., Yana, I., Ohno, H., Seiki, M., 2001. Cytoplasmic tail-dependent internalization of membrane-type 1 matrix metalloproteinase is important for its invasion-promoting activity. J. Cell Biol. 155, 1345–1356.

Voinea, M., Manduteanu, I., Dragomir, E., Capraru, M., Simionescu, M., 2005. Immunoliposomes directed toward VCAM-1 interact specifically with activated endothelial cells—a potential tool for specific drug delivery. Pharm. Res. 22, 1906–1917.

Wang, X., Ma, D., Keski-Oja, J., Pei, D., 2004. Co-recycling of MT1-MMP and MT3-MMP through the trans-Golgi network. Identification of DKV582 as a recycling signal. J. Biol. Chem. 279, 9331–9336.

Xu, L., Huang, C.C., Huang, W., Tang, W.H., Rait, A., Yin, Y.Z., Cruz, I., Xiang, L.M., Pirollo, K.F., Chang, E.H., 2002. Systemic tumor-targeted gene delivery by anti-transferrin receptor scFv-immunoliposomes. Mol. Cancer Ther. 1, 337–346.

Zhang, Y., Boado, R.J., Pardridge, W.M., 2003. Marked enhancement in gene expression by targeting the human insulin receptor. J. Gene Med. 5, 157–163.

In Vitro Efficacy of a Sterically Stabilized Immunoliposomes Targeted to Membrane Type 1 Matrix Metalloproteinase (MT1-MMP)

Kazutaka Atobe,[a] Tatsuhiro Ishida,[a] Emi Ishida,[b] Kouichi Hashimoto,[b] Hideo Kobayashi,[b] Jyunko Yasuda,[c] Takanori Aoki,[c] Ken-ichi Obata,[c] Hiroshi Kikuchi,[b] Hidetaka Akita,[d] Tomohiro Asai,[e] Hideyoshi Harashima,[d] Naoto Oku,[e] and Hiroshi Kiwada*,[a]

[a] *Department of Pharmacokinetics and Biopharmaceutics, Subdivision of Biopharmaceutical Sciences, Institute of Health Biosciences, the University of Tokushima; 1–78–1 Sho-machi, Tokushima 770–8505, Japan:* [b] *Drug Metabolism and Physicochemistry Research Laboratory, R&D Division, Daiichi Pharmaceutical Co., Ltd.; Tokyo 134–8630, Japan:* [c] *Daiichi Fine Chemical Co., Ltd.; Takaoka, Toyama 933–8511, Japan:* [d] *Graduate School of Pharmaceutical Sciences, Hokkaido University; Sapporo, Hokkaido 060–0812, Japan: and* [e] *Department of Medical Biochemistry and COE Program in the 21st Century, University of Shizuoka School of Pharmaceutical Sciences; 52–1 Yada, Shizuoka 422–8526, Japan.*

Received January 31, 2007; accepted February 14, 2007; published online March 12, 2007

The poor selective cytotoxicity of anticancer drugs lead to dose-limiting adverse effects which compromise the clinical outcome. Solid tumors recruit new blood vessels to support their growth, and epitopes that are uniquely expressed on tumor cells and tumor endothelial cells (ECs) can function as targets for immunoliposomal anticancer drugs. Membrane type 1 matrix metalloproteinase (MT1-MMP), an important protein related to tumor growth and angiogenesis, is expressed on malignant tumor cells and is activated ECs. Selective delivery could be achieved by targeting MT1-MMP, as well as other angiogenic ECs. In this regard, an anti-MT1-MMP Fab′ antibody was used to prepare a MT1-MMP targeted sterically stabilized immunoliposomes (SIL[anti-MT1-MMP(Fab′)]). The binding and intracellular distribution of SIL[anti-MT1-MMP(Fab′)] and a non-targeted sterically stabilized liposomes (SL) were examined using human fibrosarcoma HT-1080 cells. SIL[anti-MT1-MMP(Fab′)] was taken up by the cells in a lipid concentration, temperature, and time dependent manner, ultimately accumulating in the lysosomes. The cytotoxicity of doxorubicin (DXR)-containing SIL[anti-MT1-MMP(Fab′)] (DXR-SIL[anti-MT1-MMP(Fab′)]) was significantly higher than that of DXR-containing SL. The cellular internalization of SIL[anti-MT1-MMP(Fab′)] was inhibited by endocytosis inhibitors, suggesting that their internalization was mediated *via* clathrin- or caveolae-dependent endocytosis. Furthermore, the efficient binding of SIL[anti-MT1-MMP(Fab′)] was observed on human umbilical vein endothelial cells (HUVEC). Based on these results, it would be expected that DXR-SIL[anti-MT1-MMP(Fab′)] may achieve direct tumor cell kill and indirect tumor cell kill *via* the destruction of the tumor endothelium *in vivo*. This strategy may have the potential for overcoming some major limitations in conventional chemotherapy *in vivo*.

Key words immunoliposome; targeting; PEGylation; membrane type 1 matrix metalloproteinase (MT1-MMP); human umbilical vein endothelial cell (HUVEC); cellular uptake

Therapeutic approaches to cancer continue to focus on developing novel delivery systems to increase the therapeutic indices of anticancer agents by targeting drugs to diseased malignant cells and not from normal tissues. One approach uses the expression of cell surface epitopes as unique targets for the selective delivery of antibody-based therapies. The encapsulation of anticancer drugs in liposomes can alter their pharmacokinetics and biodistribution, resulting in an increased efficacy and/or decreased toxicity. Long-circulating liposome formulations containing engrafted polyethylene glycol (PEG) on their surface (sterically stabilized, PEGylated, liposomes (SL)) have recently been developed.[1—3] Doxorubicin (DXR)-containing SL (DXR-SL) has been approved in a number of countries, including Japan, for the treatment of Kaposi's sarcoma, breast, ovarian and endometrial cancer.[4—8] With the development of techniques for coupling specific ligands to the terminus of PEG,[9,10] novel approaches for the use of liposomes as homing devices for the selective targeting of anticancer drugs to malignant cells are now available. Ligand-targeted sterically stabilized liposomal drugs (sterically stabilized immunoliposomes (SIL)) that promote the selective binding of the liposomes to target cells have shown enhanced antitumor effects relative to non-targeted sterically stabilized liposomal drugs.[11]

Membrane type 1 matrix metalloproteinase (MT1-MMP), the first identified matrix proteinase in the zinc-dependent matrix metalloproteinase family, is known to be required for the degradation of the extracellular matrix (ECM), endothelial invasion and migration, the formation of capillary tubes, and the recruitment of accessory cells.[12] MT1-MMP expression has been reported to be correlated with the malignancy of multiple tumor types including lung, gastric, colon, breast, cervical carcinomas, gliomas and melanomas[13] and to play an important role in metastasis and angiogenesis.[12,14] In addition, it has been demonstrated that MT1-MMP is expressed on various tumor cells and human endothelial cells (ECs) and is internalized through the classic clathrin and dynamin-dependent endocytic pathway and/or caveolae in tumor cells[15—17] and caveolae in human ECs.[17,18] It can therefore be considered to be an excellent targeting moiety in applications involving liposome-entrapped drugs.

The targeting of liposomal drugs to the MT1-MMP moiety may achieve the selective delivery of anticancer therapeutics to, not only tumor cells, but also ECs in tumor vasculatures. This approach may show additive or synergistic antitumor effects compared with either type of targeting used alone. To investigate this approach further, we prepared a sterically stabilized immunoliposomes coupled with the Fab′ of anti-MT1-MMP mAb (SIL[anti-MT1-MMP(Fab′)] and examined in the *in vitro* efficacy of the sterically stabilized immunoli-

* To whom correspondence should be addressed. e-mail: hkiwada@ph.tokushima-u.ac.jp

posomal formulation on a human fibrosarcoma cell line, HT-1080 cells. In addition, we examined the selective binding of the liposomes to human umbilical vein endothelial cell (HUVEC) as a model of ECs of tumor vasculatures.

MATERIALS AND METHODS

Materials Hydrogenated soy phosphatidylcholine (HSPC) was purchased from Lipoid (Ludwigshafen, Germany). Cholesterol (Chol) was purchased from Wako Pure Chemical (Osaka, Japan). 1,2-Distearoyl-*sn*-glycero-3-phosphoethanolamine-*n*-[methoxy(polyethylene glycol) 2000] ($mPEG_{2000}$-DSPE) was purchased from Genzyme (MS, U.S.A.). PEG_{2600}-DSPE with a functional maleimide moiety at the terminal end of PEG: *N*-[(3-maleimide-1-oxopropyl)aminopropyl polyethyleneglycol ($_{2600}$)-carbamyl] distearoyl-ethanolamine (Mal-PEG_{2600}-DSPE) was purchased from Shearwater (Enschede, Netherlands). Doxorubicin (DXR) was purchased from Sicor, Inc. (CA, U.S.A.). Methyl-β-cyclodextrin (cdx) was purchased from Sigma (St. Louis, U.S.A.). Chlorpromazine (CPZ) was purchased from Wako Pure Chemical (Osaka, Japan).

Cell Line HT-1080 cells, a human fibrosarcoma, was purchased from Dainippon Pharmaceutical (Osaka, Japan) and maintained in DMEM (Sigma, MO, U.S.A.) containing heat-inactivated 10% fetal bovine serum (FBS, Japan Bioserum, Hiroshima, Japan), penicillin (50 U/ml) and streptomycin (50 μg/ml) at 37°C in humidified atmosphere containing 5% CO_2.

HUVEC, a human umbilical vein endothelial cell, was purchased from CAMBREX (MD, U.S.A.) and maintained in endothelial cell medium EGM-2 (CAMBREX, MD, U.S.A.) containing heat-inactivated 2% FBS, Human EGF, hydrocortisone, VEGF, Human bFGF, IGF-1, ascorbic acid, heparin, gentamicin and amphotericin-B at 37°C in humidified atmosphere containing 5% CO_2.

Flow Cytometry HT-1080 cells were detached with PBS(−) containing 0.5 mM EDTA, washed with PBS(−) by centrifugation (1000 rpm, 5 min, 4°C), and resuspended in PBS(−) containing 1% BSA. The cells were fixed with 4% paraformaldehyde for 1 h at 37°C and then washed twice with PBS(−). In some experiments, in order to increase membrane permeability, a part of the cells was incubated for 1 h at 4°C with 1% saponin (MP Biomedicals, Ohio, U.S.A.). A 0.1 ml aliquot of the HT-1080 cells suspension (5.0×10^6 cells/ml) was incubated for 1 h at 4°C with 0.1 ml of anti-MT1-MMP mAb (20 μg/ml). To remove unreacted mAb, the cells were washed twice with phosphate buffered saline (PBS(−), 1.6 mM NaH_2PO_4, 8 mM Na_2HPO_4, 2.6 mM KCl, 137 mM NaCl, pH 7.5) containing 1% BSA by centrifugation (1000 rpm, 5 min, 4°C). The cells were then further incubated with 0.1 ml of a FITC-conjugated anti-mouse IgG (20 μg/ml) for 1 h at 4°C. Finally, the sample was analyzed using Guava EasyCyte (GE Healthcare Bio-Sciences, Uppsala, Sweden).

Preparation of Anti-MT1-MMP Antibody and Fab' Fragment of the Antibody A murine monoclonal IgG antibody [222-1D8][19] was purified from ascites fluid of BALB/c mice by centrifugation (3000 rpm, 15 min, 4°C) followed by filtration of the supernatant and purification on a protein G affinity column (GE Healthcare Bio-Sciences, Uppsala, Sweden) according to the manufacturer's instructions.

For preparation of the $F(ab')_2$ fragment, the purified anti-MT1-MMP monoclonal antibody (mAb) (50 mg) was digested with 2% pepsin A (Worthington Biochemical Corporation, NJ, U.S.A.) in 0.1 M sodium acetate buffer (0.1 M sodium acetate, 0.1 M acetic acid, 0.1 M NaCl, pH 4.2) at 37°C for 22.5 h. The reaction was stopped by the addition of 300 ml of 3 M Tris–HCl buffer (pH 7.5). The reaction mixture was then passed through a Ultrogel AcA 44 (Pall corporation, NY, U.S.A.) column equilibrated with 0.1 M phosphate buffer (36 mM NaH_2PO_4, 64 mM Na_2HPO_4, pH 7.0). The protein concentration was determined by spectrophotometrically (λ=280 nm) (Shimadzu UV-1600, Shimadzu, Kyoto, Japan).

Preparation of Sterically Stabilized Liposomes (SL) and Sterically Stabilized Immunoliposomes (SIL).

1. Preparation of Conventional Liposomes Conventional liposomes were composed of HSPC : Chol at a 11.28 : 7.68 molar ratio. For fluorescently labeled liposomes, 1,1'-dioctadecyl-3,3,3',3'-tetramethylindocarbocyanine perchlorate (DiI) (Invitrogen, OR, U.S.A.) was incorporated into the lipid mixture.

In a typical preparation, the lipids, HSPC and Chol, were dissolved in chloroform and, after evaporation of the organic solvent, the resulting lipid film was hydrated in 250 mM ammonium sulfate (pH 5.5). The hydrated liposomes were sequentially extruded (Lipex Biomembranes Extruder, British Columbia, Canada) at 65°C through a series of polycarbonate filters (Whatman, Middlesex, U.K.) with pore sizes ranging from 0.4 (×1), 0.2 (×3), 0.1 (×3) and 0.08 (×3) μm to produce primarily unilamellar vesicles. Following extrusion, the external buffer was exchanged by elution through a Sephadex G-50 (GE Healthcare Bio-Sciences) column equilibrated with saline (0.9% NaCl). Liposomal size was characterized by dynamic light scattering using a NICOMP 370 HPL submicron particle analyzer (Particle Sizing System, CA, U.S.A.). The mean liposomal diameters of the extruded liposomes were in the range of 98—110 nm.

For DXR-loaded liposomes, the drug was encapsulated by remote-loading using an ammonium sulfate gradient.[20] Following extrusion, as described above, the prepared liposomes were passed through a Sephadex G-50 column equilibrated with 10% sucrose to exchange external buffer. The fractions containing the eluted liposomes were collected. The phospholipid concentration in the collected liposomes were determined using the Bartlett colorimetric assay.[21] DXR was added to the liposomes at a DXR/phospholipid ratio of 0.2 : 1 (w/w) and the resulting mixture was incubated for 1 h at 65°C. The liposome-encapsulated DXR was separated from free DXR on a Sephadex G-50 column eluted with saline. The concentration of the liposome-encapsulated DXR was determined spectrophotometrically (λ=480 nm) (Shimadzu UV-1600) following methanol extraction.

2. Preparation of Sterically Stabilized Liposomes Sterically stabilized liposomes (SL) were prepared using a post-insertion method[22,23] with minor modifications. The basic procedure involves transferring PEG-lipids into the bilayers of preformed, drug loaded liposomes using a simple incubation step, without any drug leakage, in a time- and temperature dependent manner.

PEGylation of the preformed conventional liposomes was carried out. Briefly, preformed conventional liposomes were

mixed with $mPEG_{2000}$-DSPE micelles (0.25 mM) in deoxygenated saline at a liposome/PEG-lipids ratio of 10 : 0.46 (mol/mol). The mixture was incubated at 65°C for 15 min with occasional gentle mixing. For preparing immuno-liposomes, Mal-PEG_{2600}-DSPE was added to $mPEG_{2000}$-DSPE at a 3 : 7 molar ratio as the PEG-lipid micelles were prepared. After the transfer, the liposome–micelle mixture was cooled and chromatographed over a Sepharose CL-4B (GE Healthcare Bio-Sciences) column equilibrated with saline to separate the resulting SL from non-transferred PEG-lipid micelles.

3. Preparation of Sterically Stabilized Immunoliposomes (SIL[anti-MT1-MMP(Fab')]) A Fab' fragment was prepared from the $F(ab')_2$ fragment of anti-MT1-MMP mAb (222-1D8). The resulting $F(ab')_2$ (10 mg), adjusted to a volume of 0.9 ml with 0.1 M phosphate buffer (pH 6.0), mixed with 0.1 ml of 0.1 M 2-aminoethanethiol hydrochloride (Wako), and then reduced at 37°C for 1.5 h. To remove the reducing agent, the preparation was loaded on an Ultrogel AcA 54 gel (Pall Corporation, NY, U.S.A.) column equilibrated with PBS(−) containing 5 mM EDTA (Wako). Elution of the Fab' was monitored at A280. The concentration of the resulting Fab' was determined spectrophotometrically (λ= 280 nm) (Shimadzu UV-1600).

To conjugate the Fab' fragment, Mal-PEG-lipid-introduced liposomes were mixed with the Fab' fragment (the molar ratio of the maleimide moiety and Fab' fragment was 1 : 3). After incubation for 20 h at 4°C, shielded from light in deoxygenated saline (pH 8.0), unreacted mercapto groups were blocked by adding 0.1 M *N*-ethylmaleimide (Wako): The molar ratio of the Fab' fragment and *N*-ethylmaleimide was 1 : 10. To remove free Fab' fragments, the reaction mixture was loaded on a Sepharose CL-4B (GE Healthcare Bio-Sciences) column equilibrated with 0.9% NaCl. The concentration of phospholipids and Fab' was determined by the Bartlett colorimetry assay[21] and DC protein assay (Bio-Rad, CA, U.S.A.), respectively. The amount of Fab' coupled to the liposomes was in the range of 30—50 μg of Fab' fragment/μmol phospholipid. The mean diameter (110—120 nm) was checked using a dynamic light scattering (a NICOMP 370 HPL submicron particle analyzer (Particle Sizing System)).

***In Vitro* Cell Binding/Uptake Experiment** A 0.5 ml aliquot of HT-1080 cells suspension (5.0×10^5 cells/ml) was plated in a 24-well tissue culture plate (Corning, NY, U.S.A.) and cultured for 24 h at 37°C. After pre-culture, the medium was exchanged to 0.5 ml of DiI-labeled SL or SIL[anti-MT1-MMP(Fab')] (0.1—0.8 mmol phospholipid/ml) without DXR, diluted with complete medium, and the plate was maintained at either 4°C or 37°C. In a competition experiment, 30 min before exchanging to DiI-labeled SIL[anti-MT1-MMP(Fab')], the medium was exchanged to fresh complete medium containing a 80-fold excess of free anti-MT1-MMP mAb (0.5 mg) to the Fab' coupled to SIL. In some experiments, the cells were pre-treated with several known endocytosis inhibitors: 1 μM cdx for 6 h, 10 μg/ml CPZ for 0.5 h, hypertonic concentration (0.45 M) of sucrose for 0.5 h, prior to the addition of the DiI-labeled liposomes. It is well known that cdx sequesters cholesterol, thus disrupts caveolae formation.[24—26] CPZ interacts with clathrin from the coated pits, thereby causes their loss from the surface membrane.[27,28] Hypertonic concentrations of sucrose inhibit endocytosis by impairing the formation of coated vesicles from clathrin-coated pits.[29—31] After a 1—24 h incubation with the liposomes, the cells were washed with cold PBS(−) twice and lysed in PBS(−) containing 0.2% Triton X-100 (Wako). The fluorescence intensity of the DiI in the lysate was determined using a fluorophotometer (Hitachi F-4500, Tokyo, Japan) with excitation and emission wavelengths at 545 and 570 nm, respectively. The protein concentration in the lysate was determined by a protein assay (DC protein assay (Bio-Rad, CA, U.S.A.)).

***In Vitro* Cytotoxicity Experiment** IC_{50} of various DXR-formulations was determined using an *in vitro* proliferation assay using 3-(4,5-dimethylthiazol-2-yl)-2,5-diphenyltetrazolium bromide (MTT) (Nacalai Tesque, Kyoto, Japan).[32] Briefly, 5.0×10^3 cells were plated in a 96-well plate (Becton Dickinson, NJ, U.S.A.) and incubated with the DXR formulation (free DXR, DXR-SL or DXR-SIL[anti-MT1-MMP(Fab')] at different DXR concentrations, and diluted with complete medium, for 1 h at 37°C. After removing the incubation mixture, the cells were washed twice with cold PBS(−). Fresh medium was then immediately added and the plate was incubated for an additional 47 h at 37°C. After removing the medium, 50 μl of MTT solution (5 mg/ml) was added to each well. Following a 3—4 h incubation, 150 μl of 40 mM HCl in isopropanol was added to dissolve any crystals formed in the well. The absorption of the dissolved crystals was determined on a microplate reader at 590 nm (Wallac1420 ARVOsx, PerkinElmer Life Science, MA, U.S.A.). IC_{50} was defined as the concentration of DXR encapsulated in the liposomes or the free form required to inhibit cells growth by 50%, compared to control wells without any drug.

Confocal Laser Microscopy A 0.1 ml aliquot of HT-1080 cells suspension (5.0×10^5 cells/ml) was plated in a glass base dish (35 mm, Glass 12ϕ, Asahi Technoglass, Tokyo, Japan). After pre-culturing for 24 h at 37°C, the medium was removed, and 0.1 ml of Alexa Fluor488 labeled-anti-MT1-MMP mAb (20 μg/ml complete medium) prepared with the Zenon Mouse IgG labeling kit (Invitrogen, OR, U.S.A.) or 0.1 ml of SIL[anti-MT1-MMP(Fab')] (200 μM in complete medium) was then added to the dish, followed by incubation for 1 or 12 h at 37°C. After washing twice with PBS(−), the cells were co-incubated with Syto24 (0.8 μl/2 ml of compete medium, Invitrogen) or LysoTracker Yellow (0.5 μM, Invitrogen) for a period and then visualized using a Zeiss confocal microscope equipped with an argon laser and a HeNe laser at ×20 or ×63 magnification (CarlZeiss, Jene, Germany).

RESULTS

MT1-MMP Expression and Internalization on HT-1080 Cells The expression of MT1-MMP molecules on HT-1080 cells was evaluated by flow cytometry (FACS) (Fig. 1A). The incubation of fluorescence (FITC)-labeled mAb with the cells was performed at 4°C to avoid internalization/recycling of MT1-MMP molecules. The FACS results showed that a very tiny amount of anti-MT1-MMP mAb was bound to HT-1080 cells, indicating that the level of MT1-MMP expression was relatively lower. In contrast, the binding of mAb in-

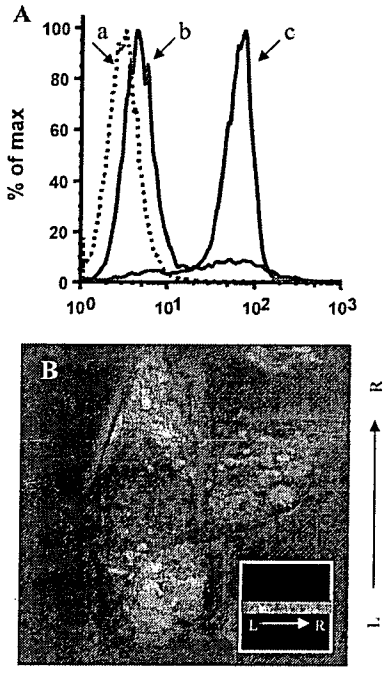

Fig. 1. MT1-MMP Expression on HT-1080 Cells

(A) MT1-MMP expression on HT-1080 cells was evaluated by FACS following incubation of the cells with fluorescent-labeled anti-MT1-MMP mAb for 1 h at 4°C. a, control; b, MT1-MMP on cell surface; c, Total MT1-MMP in cell. (B) Internalization of mAb accompanied with MT1-MMP molecules was observed by confocal microscopy following incubation of the cells with fluorescent-labeled anti-MT1-MMP mAb for 1 h at 37°C. Inserted figure represents a lateral 3D perspective of the accumulated fluorescence intensity of all slices taken by confocal microscopy (L→R).

creased when the membrane permeability was increased, indicating that a large number of MT1-MMP molecules was pooled in the subcellular compartment of the cells. In addition, an experiment was carried out to determine if the anti-MT1-MMP mAb can be internalizing accompanied with MT1-MMP molecules. The cells were incubated with mAb at 37°C for 1 h and then observed by confocal microscopy. FITC coupled to the mAb was observed inside the cells (Fig. 1B), indicating that large number of the mAb had been internalized by HT-1080 cells within 1 h. Collated confocal sections of each stack also clearly showed the internalization of the mAb (Fig. 1B, insert).

***In Vitro* Cell Binding/Uptake of Liposomes** In the range of lipid doses tested, the binding/uptake of fluorescence (DiI)-labeled targeted SL (SIL[anti-MT1-MMP(Fab')] by HT-1080 cells increased linearly with the lipid dose. In contrast, that of Ab-free liposomes (SL) was relatively lower at all lipid doses (Fig. 2A). The association of SIL[anti-MT1-MMP(Fab')] with HT-1080 cells could be competitively inhibited by approximately 40% by the addition of excess free anti-MT1-MMP mAb, indicating that the association was mediated through the MT1-MMP epitope on HT-1080 cells (Fig. 2B). The association of SIL[anti-MT1-MMP(Fab')] with HT-1080 cells increased linearly as a function of time appeared to become saturated within 12 h. In contrast, that of SL was undetectable up to 6 h and then began to increase linearly with incubation time, but this non-specific association was significantly lower than the specific association (Fig. 2C). Temperature-dependency for the association of the liposomes with HT-1080 cells was examined. In the case of SL, no temperature-dependency was observed (0.08±0.03 *vs.* 0.07±0.02). The enhanced association of SIL[anti-MT1-

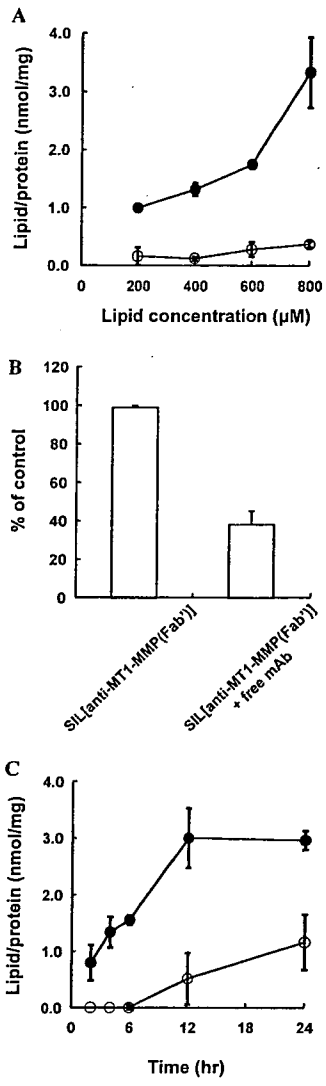

Fig. 2. Binding/Uptake of Fluorescence (DiI)-Labeled Liposomes by HT-1080 Cells

(A) Liposomes (SIL[anti-MT1-MMP(Fab')] (●) or SL (○)) with various lipid concentrations were incubated with HT-1080 cells at 37°C for 2 h. (B) SIL[anti-MT1-MMP(Fab')] (100 μM) was incubated with HT-1080 cells at 37°C for 1 h in the presence or absence of an excess of free anti-MT1-MMP mAb. (C) Liposomes (SIL[anti-MT1-MMP(Fab')] (●) or SL (○) (200 μM)) were incubated with HT-1080 cells at 37°C for indicated time period. The amount of liposome associated by the cells was determined with fluorophotometry. Each result represents the mean±S.D. of three independent experiments.

MMP(Fab')] observed at 37°C was dramatically reduced at 4°C (1.55±0.01 *vs.* 0.75±0.08) (Fig. 3A), suggesting that ATP are required for the uptake of SIL[anti-MT1-MMP(Fab')] by HT-1080 cells. Confocal microscopic pictures clearly demonstrated the internalization of SIL[anti-MT1-MMP(Fab')] in HT-1080 cells as the anti-MT1-MMP mAb was internalized (Fig. 3B). These findings indicate that Fab' coupled to liposomes triggers the internalization of liposomes by HT-1080 cells, resulting in the rapid and enhanced uptake of liposomes compared to Ab-free SL.

Internalization Pathway of SIL[anti-MT1-MMP(Fab')] in HT-1080 Cells In order to assess the mechanism involved in the uptake of SIL[anti-MT1-MMP(Fab')], HT-1080 cells were exposed to various inhibitors, which are known to affect a specific endocytotic pathway, prior to incubation with the liposomes. As shown in Fig. 4, pretreatment with CPZ and cdx reduced the uptake of the targeted liposomes by

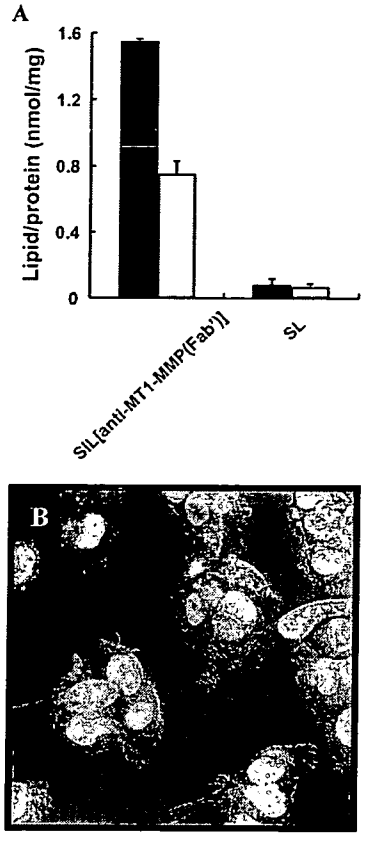

Fig. 3. Temperature-Dependency on Binding/Uptake of Fluorescence (DiI)-Labeled Liposomes by HT-1080 Cells

(A) Association of liposomes (SIL[anti-MT1-MMP(Fab')] or SL) with HT-1080 cells was determined following 2 h-incubation at either 37°C (closed column) or 4°C (open column). (B) Association of SIL[anti-MT1-MMP(Fab')] with HT-1080 cells was observed by confocal microscopy following a 2 h-incubation at 37°C. Red, SIL[anti-MT1-MMP(Fab')]; Green, Syto24 (nuclear marker).

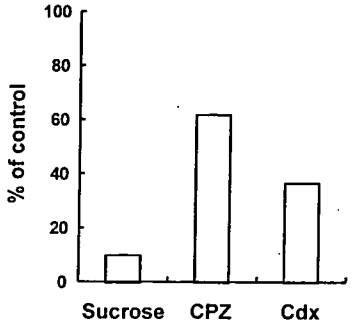

Fig. 4. Effect of Various Endocytic Inhibitors on Uptake of Fluorescence (DiI)-Labeled SIL[anti-MT1-MMP(Fab')] by HT-1080 Cells

Prior to incubation with SIL[anti-MT1-MMP(Fab')], HT-1080 cells were pre-treated at 37°C with the following endocytosis inhibitors: methyl-β-cyclodextrin (cdx, 1 μM) for 6 h, chlorpromazine (CPZ, 10 μg/ml) for 0.5 h, hypertonic concentration of sucrose (0.45 M) for 0.5 h. The association of the liposome was then determined following 6 h-incubation at 37°C.

approximately 40% and 60%, respectively. Exposure of the cells to a hypertonic concentration of sucrose also strongly inhibited the uptake of the targeted liposomes. Accordingly, SIL[anti-MT1-MMP(Fab')] seemed to be internalized into HT-1080 cells through clathrin-dependent endocytosis and caveolae. The intracellular distribution of SIL[anti-MT1-MMP(Fab')] after internalization was visualized by confocal microscopy. Confocal sections showed that SIL[anti-MT1-MMP(Fab')] was localized within the lysosomal compartment, as visualized with LysoTracker Yellow, after a 12 h-incubation (Fig. 5).

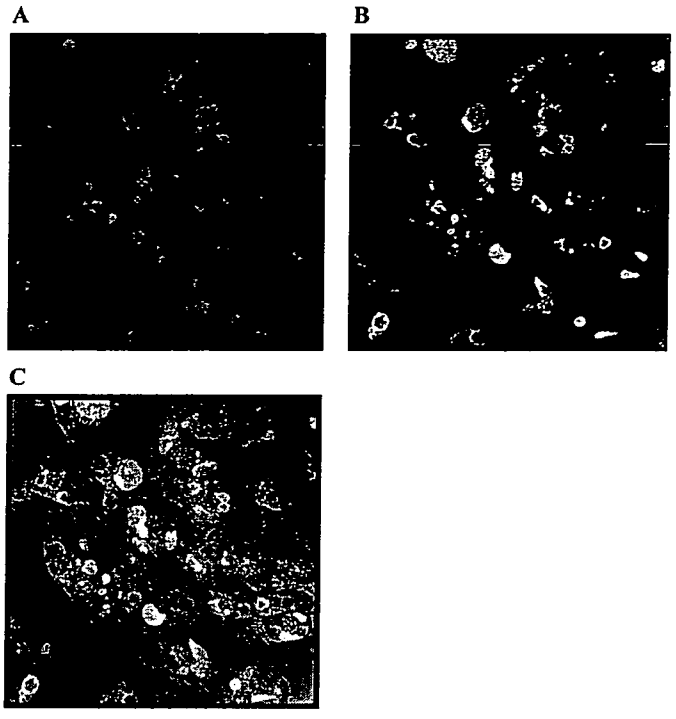

Fig. 5. Intracellular Distribution of Fluorescence (DiI)-Labeled SIL[anti-MT1-MMP(Fab')] in HT-1080 Cells

The intracellular distribution of SIL[anti-MT1-MMP(Fab')] in HT-1080 cells was visualized by using confocal microscopy following a 12 h-incubation. (A) Red, SIL[anti-MT1-MMP(Fab')]; (B) yellow, LysoTracker Yellow (lysosome); (C) merged.

Table 1. Comparison of the Cytotoxicity of Various Liposomal Formulations with DXR in HT-1080 Cells

Formulations	IC_{50} (DXR μM)
Free DXR	2.6±1.2
DXR-SL	>300
DXR-SIL[anti-MT1-MMP(Fab')]	37.5±3.1

Cytotoxicity of Doxorubicin (DXR) Formulations in HT-1080 Cells The cytotoxicity of DXR, either free or encapsulated in SL or SIL[anti-MT1-MMP(Fab')], was examined (Table 1). After a 1 h incubation, SIL[anti-MT1-MMP(Fab')] showed an approximately 9-fold higher cytotoxicity compared to non-targeted SL. This suggests that the binding and/or internalization of the targeted liposomes contribute to the increased cytotoxicity of the encapsulated DXR. However, targeted liposomal formulation was significantly less cytotoxic than the free drug *in vitro*. Additional control experiments were conducted to exclude the possibility that the cytotoxic effect may have been due to either the lipid, Fab', or a combination of both. Free Fab' (18.6 μg), drug-free SL (1.12 mM phospholipids, 300 μM DXR, if the drug was encapsulated), and drug-free SIL[anti-MT1-MMP(Fab')] (18.6 μg Fab', 1.12 mM phospholipids, 300 μM DXR if the drug was encapsulated) showed no cytotoxicity (data not shown).

Binding/Uptake of SIL[anti-MT1-MMP(Fab')] on HUVEC The association of SIL[anti-MT1-MMP(Fab')] with HUVEC, a model of ECs, was also examined. A signifi-

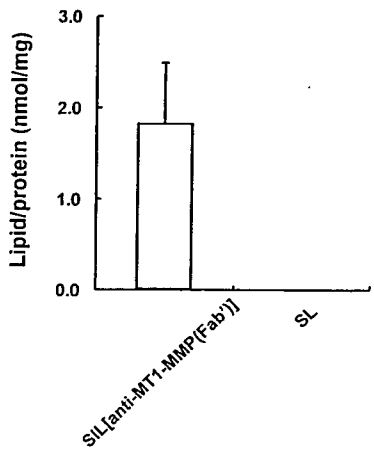

Fig. 6. Binding/Uptake of Fluorescence (DiI)-Labeled Liposomes by HUVEC

Liposomes (SIL[anti-MT1-MMP(Fab')] or SL (200 μM)) were incubated with HUVEC at 37°C for 24 h. The amount of liposome associated with the cells was determined by fluorophotometry. Each result represents the mean±S.D. of three independent experiments.

cant association was observed with the targeted liposomes, whereas minimum association (under detection limit) was observed with non-targeted liposomes (Fig. 6), suggesting that the SIL[anti-MT1-MMP(Fab')] targeted to MT1-MMP may have the ability to selectively deliver the encapsulated drugs to ECs in the tumor vasculature.

DISCUSSION

Immunoliposomes coupled with the Fab' of murine mAb against MT1-MMP, SIL[anti-MT1-MMP(Fab')], selectively bound to HT-1080 cells in a dose, time and temperature dependent manner (Figs. 2, 3). This indicates that the liposomes were internalized by the cells, along with the internalization of the MT1-MMP epitopes, following binding to target cells through Ab-epitope interactions. Many studies have shown that targeting immunoliposomal anticancer drugs to internalizing epitopes leads to the efficient entry of a drug into target cells, resulting in an increased therapeutic effect.[33—37] Although MMP would be expected to be a molecular target for preventing tumor metastasis, initial clinical tests of broad spectrum-MMP inhibitors have been disappointing.[38] However, our results suggest that, in terms of an epitope for drug delivery system, MT1-MMP is still a good targeting epitope, in terms of achieving an increased selective delivery of anticancer drugs.

From the confocal microscopic study, the internalized SIL[anti-MT1-MMP(Fab')] ultimately accumulates within the lysosomal compartment (Figs. 3B, 5). It would appear that the internalization of SIL[anti-MT1-MMP(Fab')] proceeds through clathrin-dependent endocytosis and caveolae (Fig. 4). This internalization mechanism is similar to that of MT1-MMP itself, as reported earlier.[15—17] It is assumed that the gradual breakdown of the drug package within the endocytic apparatus and the subsequent release of drug into cytoplasm may result in increased *in vivo* cytotoxicity.

In the case of a free drug, its large volume of distribution and rapid redistribution quickly lower the plasma drug levels, resulting in the exposure of target cells to only low drug levels. In contrast, non-targeted SL is capable of delivering large amounts of a drug to tumor tissue due to an enhanced permeability and retention (EPR) effect.[39,40] However, because the SL does not attach to vascular ECs, the uptake of the released drug by ECs would be low. If liposomes became attached to vascular ECs *via* a non-internalizing epitope, high local concentrations of a drug might be achieved at the outer surface of target cells. However, only a fraction of the released drug might be delivered to the target cells, depending on the rate of drug release and/or the rate of diffusion of the released drug from the cell surface. Thus, targeting to an internalized epitope is required to deliver anticancer drugs to vascular ECs. In this study, we were able to demonstrate the selective binding and possibly the internalization of SIL[anti-MT1-MMP(Fab')] in HUVEC, a model of ECs (Fig. 6). Since SIL[anti-MT1-MMP(Fab')] has extensive opportunities to come into contact with ECs of angiogenic vessels before extravasation from the tumor vasculature due to the EPR effect, formulations containing anticancer drugs may show excellent antitumor activity by killing angiogenic blood vessels and, indirectly, the tumor cells that these vessels support (anti-angiogenic therapy).

The amount of MT1-MMPs expressed on membranes of the HT-1080 cell line was relatively much lower than the amount that was subcellularly localized in the cells (Fig. 1A). However, the binding/uptake of SIL[anti-MT1-MMP(Fab')] increased with incubation time and dose, and became saturated within 12 h (Fig. 2B). This might be due to the trafficking of free MT1-MMP molecules pooled in the subcellular compartment to the cell membranes. In addition, Wang *et al.*[41] recently reported that MT1-MMP is internalized and routed through the recycling pathway back to the cell surface within 60 min. This may also account for the relative higher binding/uptake of targeted liposomes, in that the recycling of once internalized MT1-MMP molecules accompanied by the liposomes contribute to the further internalization of the liposomes.

Tumor ECs are increasingly accepted as a valid target for cancer therapy, since angiogenesis is a critical event for the maintenance, proliferation and metastasis of tumors.[42,43] MT1-MMP expression has been reported to be correlated with the invasiveness and malignancy of multiple tumor types including lung, gastric, colon, breast, cervical carcinomas, gliomas, melanomas[13] and ECs of the angiogenesis vasculature.[17,18] Therefore, SIL[anti-MT1-MMP(Fab')] containing DXR may cause antitumor activity by the selective killing of tumor endothelial cells and the destruction of the tumor vasculature as well as killing tumor cells. Straubinger *et al.*[44] clearly showed that a combination of multiple carrier-based therapies followed by treatment with angiogenic agents may represent an important and novel strategy for enhancing the efficacy of antitumor treatments. In addition, Pastorino *et al.*[45] demonstrated that dual immunoliposomal formulations, targeted to tumor cells *via* ligands against tumor-associated antigens and targeted to the tumor vasculature *via* ligands that are selectively directed against tumor endothelial cells, have additive effects in a murine neuroblastoma model compared with either therapy used alone, when used in combination in a temporal sequence. Since our immunoliposomes, SIL[anti-MT1-MMP(Fab')], is capable of both tumor-targeted and vascular-targeted therapies with a single liposomal anticancer drug formulation, a therapeutic approach with this

immunoliposomes may have further advantages. The potential for dual action induced by our immunoliposomes may result in a higher and more durable anticancer effect than a strictly anti-angiogenic approach with a simple dosing scheme.

The immunogenicity of therapeutic agents that are based on murine mAb has been a major barrier to successful therapy in humans because they evoke human anti-mouse Abs, mediated in part by the Fc region of the molecule.[46—48] In the case of immunoliposomes, this can result in an enhanced removal of the liposomes by cells of the mononuclear phagocyte system *via* Fc receptors on macrophages.[49,50] Any decrease in the circulation half-lives of the liposomes due to nonspecific uptake mechanisms will compromise their selective accumulation in target tissues. In this study, we employed an antibody fragment, Fab′ to overcome the general limitation of immunoliposomes coupled with whole Ab. Removal of the Fc domain will help the liposomes evade uptake by Fc receptors on macrophages and reduce the immunogenicity of the liposomes. This approach would increase the circulation time of the immunoliposomes and thereby increase both the degree of tumor localization and the opportunity to encounter ECs of the liposomes,[51,52] when the liposomes are intravenously injected.

In conclusion, sterically stabilized immunoliposomes targeted to MT1-MMP that possibly delivers anticancer drugs to both ECs in blood vessels and to tumor cells, with less-immunogeneicity and long-circulating properties ware prepared. This liposome may be a useful anticancer drug-carrier for a novel tumor treatment strategy.

Acknowledgement The authors thank Dr. Milton S. Feather for helpful advice concerning the English in this manuscript.

REFERENCES

1) Allen T. M., Mehra T., Hansen C., Chin Y. C., *Cancer Res.*, **52**, 2431—2439 (1992).
2) Gabizon A., Catane R., Uziely B., Kaufman B., Safra T., Cohen R., Martin F., Huang A., Barenholz Y., *Cancer Res.*, **54**, 987—992 (1994).
3) Allen T. M., Hansen C. B., Lopez de Menzes D. E., *Adv. Drug Del. Rev.*, **16**, 267—284 (1995).
4) Northfelt D. W., Martin F. J., Working P., Volberding P. A., Russell J., Newman M., Amantea M. A., Kaplan L. D., *J. Clin. Pharmacol.*, **36**, 55—63 (1996).
5) Lyass O., Uziely B., Ben-Yosef R., Tzemach D., Heshing N. I., Lotem M., Brufman G., Gabizon A., *Cancer*, **89**, 1037—1047 (2000).
6) O'Brien M. E., Wigler N., Inbar M., Rosso R., Grischke E., Santoro A., Catane R., Kieback D. G., Tomczak P., Ackland S. P., Orlandi F., Mellars L., Alland L., Tendler C., *Ann. Oncol.*, **15**, 440—449 (2004).
7) Muggia F. M., Hainsworth J. D., Jeffers S., Miller P., Groshen S., Tan M., Roman L., Uziely B., Muderspach L., Garcia A., Burnett A., Greco F. A., Morrow C. P., Paradiso L. J., Liang L. J., *J. Clin. Oncol.*, **15**, 987—993 (1997).
8) Gordon A. N., Granai C. O., Rose P. G., Hainsworth J., Lopez A., Weissman C., Rosales R., Sharpington T., *J. Clin. Oncol.*, **18**, 3093—3100 (2000).
9) Allen T. M., Brandeis E., Hansen C. B., Kao G. Y., Zalipsky S., *Biochim. Biophys. Acta*, **1237**, 99—108 (1995).
10) Hansen C. B., Kao G. Y., Moase E. H., Zalipsky S., Allen T. M., *Biochim. Biophys. Acta*, **1239**, 133—144 (1995).
11) Allen T. M., *Nat. Rev. Cancer*, **2**, 750—763 (2002).
12) Genis L., Galvez B. G., Gonzalo P., Arroyo A. G., *Cancer Metastasis Rev.*, **25**, 77—86 (2006).
13) Yana I., Seiki M., *Clin. Exp. Metastasis*, **19**, 209—215 (2002).
14) Sato H., Takino T., Miyamori H., *Cancer Sci.*, **96**, 212—217 (2005).
15) Jiang A., Lehti K., Wang X., Weiss S. J., Keski-Oja J., Pei D., *Proc. Natl. Acad. Sci. U.S.A.*, **98**, 13693—13698 (2001).
16) Uekita T., Itoh Y., Yana I., Ohno H., Seiki M., *J. Cell Biol.*, **155**, 1345—1356 (2001).
17) Remacle A., Murphy G., Roghi C., *J. Cell Sci.*, **116**, 3905—3916 (2003).
18) Galvez B. G., Matias-Roman S., Yanez-Mo M., Vicente-Manzanares M., Sanchez-Madrid F., Arroyo A. G., *Mol. Biol. Cell*, **15**, 678—687 (2004).
19) Aoki T., Yonezawa K., Ohuchi E., Fujimoto N., Iwata K., Shimada T., Shiomi T., Okada Y., Seiki M., *J. Immunoassay Immunochem.*, **23**, 49—68 (2002).
20) Bolotin E. M., Cohen R., Bar L. K., Emanuel N., Nisio S., Lasic D. D., Barenholz Y., *J. Liposome Res.*, **4**, 455—479 (1994).
21) Bartlett G. R., *J. Biol. Chem.*, **234**, 466—468 (1959).
22) Uster P. S., Allen T. M., Daniel B. E., Mendez C. J., Newman M. S., Zhu G. Z., *FEBS Lett.*, **386**, 243—246 (1996).
23) Ishida T., Iden D. L., Allen T. M., *FEBS Lett.*, **460**, 129—133 (1999).
24) Rodal S. K., Skretting G., Garred O., Vilhardt F., van Deurs B., Sandvig K., *Mol. Biol. Cell*, **10**, 961—974 (1999).
25) Subtil A., Gaidarov I., Kobylarz K., Lampson M. A., Keen J. H., McGraw T. E., *Proc. Natl. Acad. Sci. U.S.A.*, **96**, 6775—6780 (1999).
26) Thomsen P., Roepstorff K., Stahlhut M., van Deurs B., *Mol. Biol. Cell*, **13**, 238—250 (2002).
27) Wang L. H., Rothberg K. G., Anderson R. G., *J. Cell Biol.*, **123**, 1107—1117 (1993).
28) Orlandi P. A., Fishman P. H., *J. Cell Biol.*, **141**, 905—915 (1998).
29) Silverstein S. C., Steinman R. M., Cohn Z. A., *Annu. Rev. Biochem.*, **46**, 669—722 (1977).
30) Sandvig K., Olsnes S., *J. Biol. Chem.*, **257**, 7504—7513 (1982).
31) Sandvig K., Olsnes S., Brown J. E., Petersen O. W., van Deurs B., *J. Cell Biol.*, **108**, 1331—1343 (1989).
32) Mosmann T., *J. Immunol. Methods*, **65**, 55—63 (1983).
33) Lopes de Menezes D. E., Pilarski L. M., Allen T. M., *Cancer Res.*, **58**, 3320—3330 (1998).
34) Kirpotin D. B., Drummond D. C., Shao Y., Shalaby M. R., Hong K., Nielsen U. B., Marks J. D., Benz C. C., Park J. W., *Cancer Res.*, **66**, 6732—6740 (2006).
35) Drummond D. C., Hong K., Park J. W., Benz C. C., Kirpotin D. B., *Vitam. Horm.*, **60**, 285—332 (2000).
36) Kobayashi T., Ishida T., Okada Y., Ise S., Harashima H., Kiwada H., *Int. J. Pharm.*, **329**, 94—102 (2007).
37) Iinuma H., Maruyama K., Okinaga K., Sasaki K., Sekine T., Ishida O., Ogiwara N., Johkura K., Yonemura Y., *Int. J. Cancer*, **99**, 130—137 (2002).
38) Overall C. M., Kleifeld O., *Br. J. Cancer*, **94**, 941—946 (2006).
39) Matsumura Y., Maeda H., *Cancer Res.*, **46**, 6387—6392 (1986).
40) Muggia F. M., *Clin. Cancer Res.*, **5**, 7—8 (1999).
41) Wang X., Ma D., Keski-Oja J., Pei D., *J. Biol. Chem.*, **279**, 9331—9336 (2004).
42) Folkman J., D'Amore P. A., *Cell*, **87**, 1153—1155 (1996).
43) O'Reilly M. S., Holmgren L., Chen C., Folkman J., *Nat. Med.*, **2**, 689—692 (1996).
44) Straubinger R. M., Arnold R. D., Zhou R., Mazurchuk R., Slack J. E., *Anticancer Res.*, **24**, 397—404 (2004).
45) Pastorino F., Brignole C., Di Paolo D., Nico B., Pezzolo A., Marimpietri D., Pagnan G., Piccardi F., Cilli M., Longhi R., Ribatti D., Corti A., Allen T. M., Ponzoni M., *Cancer Res.*, **66**, 10073—10082 (2006).
46) Schroff R. W., Foon K. A., Beatty S. M., Oldham R. K., Morgan A. C., Jr., *Cancer Res.*, **45**, 879—885 (1985).
47) Phillips N. C., Dahman J., *Immunol. Lett.*, **45**, 149—152 (1995).
48) Carter P., *Nat. Rev. Cancer*, **1**, 118—129 (2001).
49) Maruyama K., Holmberg E., Kennel S. J., Klibanov A., Torchilin V. P., Huang L., *J. Pharm. Sci.*, **79**, 978—984 (1990).
50) Harding J. A., Engbers C. M., Newman M. S., Goldstein N. I., Zalipsky S., *Biochim. Biophys. Acta*, **1327**, 181—192 (1997).
51) Maruyama K., Takahashi N., Tagawa T., Nagaike K., Iwatsuru M., *FEBS Lett.*, **413**, 177—180 (1997).
52) Pastorino F., Brignole C., Marimpietri D., Sapra P., Moase E. H., Allen T. M., Ponzoni M., *Cancer Res.*, **63**, 86—92 (2003).

Biol. Pharm. Bull. 30(12) 2300—2307 (2007) Vol. 30, No. 12

Proteomic Characterization of Angiogenic Endothelial Cells Stimulated with Cancer Cell-Conditioned Medium

Yasufumi KATANASAKA,[a,c] Tomohiro ASAI,[a,c] Hirotaka NAITOU,[b,c] Norio OHASHI,[b,c] and Naoto OKU*,[a,c]

[a] *Department of Medical Biochemistry, School of Pharmaceutical Sciences, University of Shizuoka;* [b] *Graduate School of Nutritional and Environmental Sciences, University of Shizuoka; and* [c] *Global COE, University of Shizuoka; 52–1 Yada, Suruga-ku, Shizuoka 422–8526, Japan.* Received August 17, 2007; accepted September 14, 2007

To characterize the protein expression profiles and identify the molecules associated with tumor angiogenesis, the cellular proteins of human umbilical vein endothelial cells (HUVECs) in response to cancer cell-conditioned medium (CM) prepared from HT1080 human fibrosarcoma cells were analyzed using fluorescence-labeled 2D gel-based proteomics. Most differentially expressed proteins in HT1080-CM-stimulated cells were found to be downregulated (88%) rather than upregulated (12%) based on statistical analysis of protein spot signals. Additionally, we examined the effects of vascular endothelial cell growth factor (VEGF), a proangiogenic factor, on cellular protein expression. In contrast, most differentially expressed proteins were found to be upregulated (59%) rather than downregulated (41%) in VEGF-stimulated HUVECs. Comparative analyses of 29 and 35 protein species identified in CM-stimulated and VEGF-stimulated HUVECs, respectively, revealed the remarkable differences between these two stimulations. Only four proteins were differentially expressed by both treatments: annexin A2, enolase 1, and T-plastin (downregulated by CM but upregulated by VEGF), and RAN (downregulated by both CM and VEGF). These findings provide new information regarding the regulation of protein expression associated with tumor angiogenesis.

Key words: tumor angiogenesis; cancer cell-conditioned medium; proteomics; vascular endothelial cell growth factor; two-dimensional difference gel electrophoresis

Angiogenesis, the development of neovessels from preexisting blood vessels, occurs in various pathologic conditions such as diabetes, rheumatism, and cancer.[1] The processes of tumor angiogenesis is initiated through activation of endothelial cells (ECs) by proangiogenic factors such as vascular endothelial cell growth factor (VEGF) and basic fibroblast growth factor (bFGF). Then, ECs degrade the extracellular matrix (ECM) by secreting matrix metalloproteinases and invade through the ECM. Eventually, ECs proliferate and migrate to construct neovessels.[2] Tumor angiogenesis occurs through complex processes based on the interaction of ECs with surrounding cells such as tumor cells, fibroblasts, stromal cells, and macrophages. Tumor endothelium modulates the expression of various molecules such as VEGF receptor and integrins.[3]

VEGF is widely studied for understanding angiogenic mechanisms.[4] VEGF-regulated cellular molecules have been partially characterized by DNA microarray[5] or proteomic analysis using conventional two-dimensional electrophoresis (2-DE).[6] Because cancer cells produce multiple proangiogenic factors and angiogenic inhibitors,[2] cancer cell-conditioned medium (CM) rather than VEGF alone is expected to induce changes in ECs more similar to actual tumor angiogenesis *in vitro*. However, the cellular proteins associated with CM-induced angiogenesis have not been well characterized.

The proteomic approach is a powerful tool to identify protein molecules useful for biomarkers or therapeutic targets and to better understand protein–protein interactions.[7,8] Fluorescence-prelabeled two-dimensional difference gel electrophoresis (2D-DIGE) can analyze multiple protein samples in a single gel and it has higher sensitivity, reproducibility, and quantitative accuracy than conventional 2-DE.[9]

In this study, we characterized the protein expression profiles and identified the protein molecules of human umbilical vein endothelial cells (HUVECs) in response to stimulation with CM prepared from the human fibrosarcoma cell line HT1080 using 2D-DIGE and matrix-assisted laser desorption/ionization tandem time of flight mass spectrometry (MALDI-TOF/TOF-MS). In addition, we conducted proteomics using VEGF-stimulated HUVECs and analyzed the difference between CM-induced and VEGF-induced changes at the protein molecule level.

MATERIALS AND METHODS

Cell Culture and Preparation of CM HUVECs purchased from Cambrex Corporation were cultured in endothelial cell growth medium (EGM, Cambrex Corporation, Walkersville, MD, U.S.A.). Human fibrosarcoma HT1080 cells were cultured in RPMI 1640 medium supplemented with heat-inactivated 10% fetal bovine serum. To prepare CM, HT1080 cells were cultured to subconfluence, and then the medium was changed to endothelial basal medium (EBM, Cambrex Corporation). After incubation for 24 h, the culture medium was collected, centrifuged at 500×***g*** for 10 min, filtrated to remove the cell debris, and used as CM for the following experiments.

Cell Proliferation Assay HUVECs (3×10^4 cells) were seeded and incubated for 24 h. After the medium was changed to EBM (untreated) or HT1080-CM (treated), the cells were further incubated for 48 h. Viable cell density was determined with the crystal violet staining method: The viable cells were stained with 0.1% crystal violet for 15 min. After washing, the dye extracted with 33% acetic acid was measured with absorption at 570 nm.

Tube Formation Assay Growth factor-reduced Matrigel (BD Biosciences, San Diego, CA, U.S.A.) was added to 24-well plates and incubated for 30 min. HUVECs (5×10^4 cells) were seeded in EBM (untreated) or HT1080-CM (treated) on the matrigel-coated plates, and incubated for 18 h. The mi-

* To whom correspondence should be addressed. e-mail: oku@u-shizuoka-ken.ac.jp

croscopic images were scanned using Penguin Mate software (Pixera Corporation). The degree of tube formation was quantified by measuring the tube length in six randomly chosen fields using ImageJ software.

Sample Preparation for 2D-DIGE HUVECs were cultured to subconfluence, and then the medium was changed to EBM or HT1080-CM. The cells were further incubated for 24 h. In another experiment, HUVECs were cultured in EBM with or without recombinant human $VEGF_{165}$ (20 ng/ml, BD Biosciences) for 48 h. After incubation, the respective cells were harvested and solubilized with lysis buffer (7 M urea, 2 M thiourea, 4% CHAPS, 30 mM Tris–HCl (pH 8.5)) containing complete protease inhibitor cocktail (Roche Molecular Biochemicals, Indianapolis, IN, U.S.A.). Those cell lysates were centrifuged at 340,000×*g* for 30 min to remove insoluble materials, and the obtained supernatants were dialyzed with a mini dialysis kit (GE Healthcare UK Ltd.) according to manufacturer's recommended protocol. Protein concentration was determined with the Bradford protein assay method (Bio-Rad Laboratories).

2D-DIGE 2D-DIGE was performed following the procedure as described previously.[10] In brief, the extracted proteins were fluorescently labeled with three cyanine dyes, Cy2 (a pooled sample as an internal standard (treated : untreated = 1 : 1)), Cy3 (untreated HUVECs), and Cy5 (CM- or VEGF-treated HUVECs), respectively. The protein samples were incubated for 30 min on ice, and then 10 mM of lysine was added to each sample to quench the reaction. The labeled samples were mixed and used for 2-DE. The first separation was performed with the IPGphor system (GE Healthcare) using IPG strips (pH3-10NL, 24 cm). The IPG strips were rehydrated with CyDye-labeled samples at 20 °C for 12 h, and isoelectric focusing (IEF) was performed to a total of 80 kV h with IPGphor at 20 °C. The IPG strips were equilibrated for 15 min in equilibration buffer (6 M urea, 30% glycerol, 2% SDS, 50 mM Tris–HCl (pH 8.8) and 10 mg/ml of DTT) and then for 15 min in the same buffer containing 25 mg/ml of iodoacetamide instead of DTT. The equilibrated strips were transferred onto 10% polyacrylamide gel and the gels were electrophoresed.

Image Analysis The 2D-gel images were scanned using a Typhoon 9400 scanner (GE Healthcare) and statistically analyzed with DyCyder software (version 5.0; GE Healthcare). Protein spots that had been abundantly changed above 1.5 or below 0.67 between treated and untreated samples were defined as picking proteins of interest.[8]

Spot Picking and In-Gel Digestion For spot picking, a large amount of protein samples (*ca.* 500 μg) without fluorescent prelabeling was subjected to 2-DE, and the gel was stained with DeepPurple (GE Healthcare). Protein spots of interest were picked with Ettan Spotpicker (GE Healthcare). The gel pieces picked were destained with 50 mM ammonium bicarbonate/50% acetonitrile (ACN) and dehydrated with ACN. Then, the dried gel pieces were treated with trypsin solution (25 ng/ml) overnight at 37 °C. The digested peptides were extracted from the gel pieces with 80% ACN/1% trifuluoroacetic acid (TFA) and concentrated with vacuum centrifugation.

MALDI-TOF/TOF-MS Analysis The peptide solutions were desalted and concentrated with Zip-Tip C18μ (Millipore, Bedford, MA, U.S.A.). Then, the samples were mixed with α-cyano-4-hydroxycinnamic acid and applied onto target plates. MS/MS spectra were obtained using Ultraflex (Bruker Daltonics, Bremen, Germany) in reflector mode and analyzed with flexanalysis software (Bruker Daltonics). Protein identification was carried out with Mascot software against the database of the NCBI.

RESULTS

Proliferation and Tube Formation of HUVECs Stimulated with CM We first examined the effect of CM on the cellular proliferation and tube formation activities of ECs. The HT1080-CM-treated HUVECs significantly proliferated compared with untreated HUVECs (Fig. 1A), and accelerated the formation of tube-like structures (Fig. 1B, C). These results suggest that the molecular changes in HT1080-CM-stimulated HUVECs can be expected to reflect the conditions

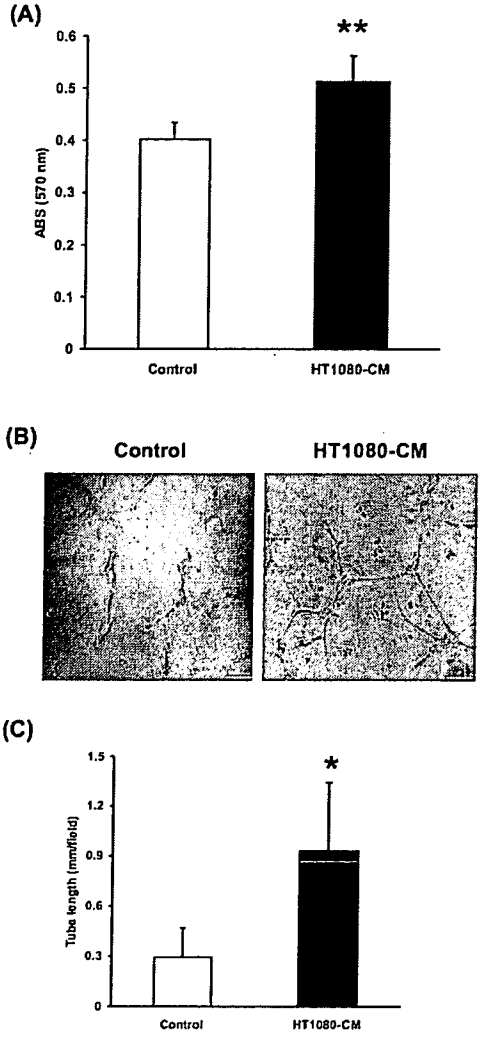

Fig. 1. Effects of HT1080 Cell-Conditioned Medium on Cell Proliferation and Tube Formation of HUVECs

(A) HUVECs were seeded (3×10^4 cells) and incubated for 24 h. After the medium was changed to EBM (control) or HT1080-CM, the cells were further incubated for 48 h. Then, the cells were stained with crystal violet and viable cell density was determined as described in Materials and Methods. Similar results were obtained at least three times independent experiments. (B) HUVECs were seeded (5×10^4 cells/well) on matrigel-coated 24-well plates in EBM or HT1080-CM, and tube formation assay was performed as described in Materials and Methods. Scale bar indicates 100 μm. (C) The tube length (μm/field) was quantified with ImageJ software. Data indicate the mean±S.D., and statistical analysis was performed with Student *t*-test. Significant differences are indicated: $*p<0.05$; $**p<0.01$.

of actual tumor angiogenesis to some extent.

Characterization of Protein Expression Profiles and Identification of Differentially Expressed Proteins in Response to CM Stimulation We performed proteomic analysis of HT1080-CM-treated HUVECs using 2D-DIGE to characterize the expression profiles and identify protein species associated with CM-induced angiogenesis. The 2D-gel images of the cellular proteins are shown in Fig. 2.

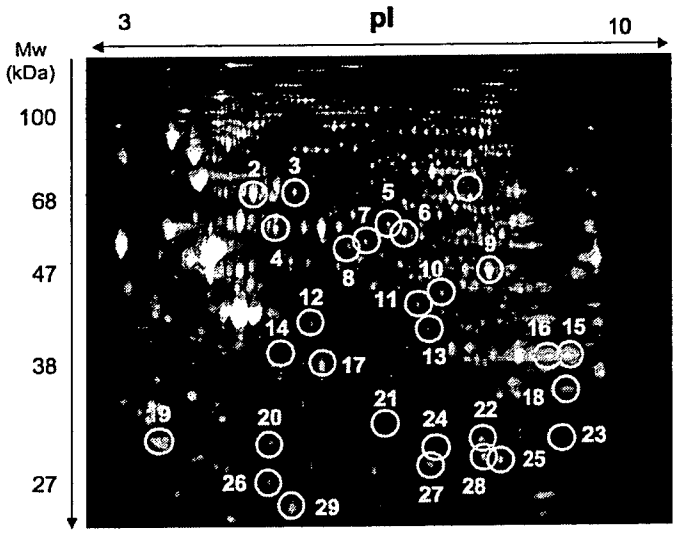

Fig. 2. Differentially Expressed Protein Profile in HUVECs Treated with HT1080-CM

Untreated HUVECs (control) and HT1080-CM-treated HUVECs were solubilized, and the extracted proteins were labeled with CyDye (Cy3: control, Cy5: HT1080-CM-treated). Pooled sample (internal standard) was labeled with Cy2. Red spots show the protein species upregulated in expression, and green spots show those downregulated in expression by the treatment with HT1080-CM. Spot numbers correspond to those in Table 1.

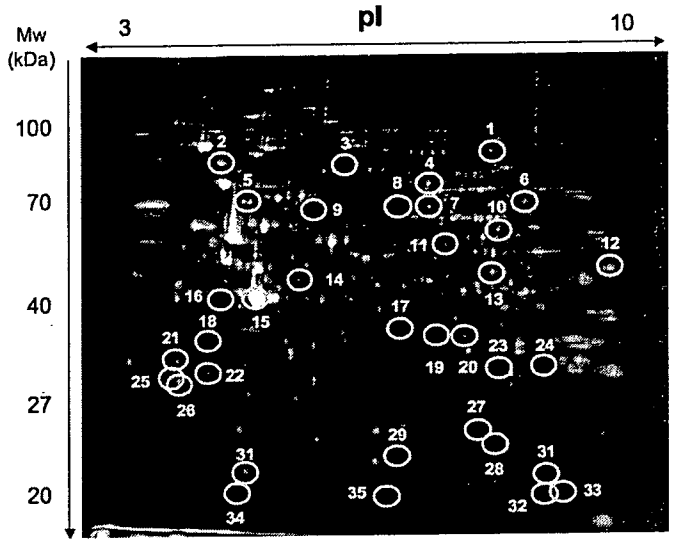

Fig. 5. Differentially Expressed Protein Profile in HUVECs Treated with VEGF

HUVECs stimulated with VEGF (20 ng/ml) were lysed, and the extracted proteins from the cells were labeled with CyDye (Cy3: control, Cy5: VEGF). Pooled sample (internal standard) was labeled with Cy2. Red spots show proteins upregulated in expression, and green spots show those downregulated in expression by treatment with VEGF. Spot numbers correspond to those in Table 2.

(A)

Observed	Mr (expt)	Mr (calc)	Delta	Start	End	Miss	Peptide
922.504	921.497	921.457	0.04	109	115	0	NVPNWHR
1294.631	1294.631	1293.623	0.0243	70	80	0	FNVWDTAGQEK
1784.904	1784.904	1783.897	-0.0079	162	175	0	SNYNFEKPFLWLAR
2052.083	2052.083	2051.075	-0.0199	48	65	0	YVATLGVEVHPLVFHTNR
2180.134	2180.154	2179.146	-0.0438	47	65	1	KYVATLGVEVHPLVFHTNR

(B)

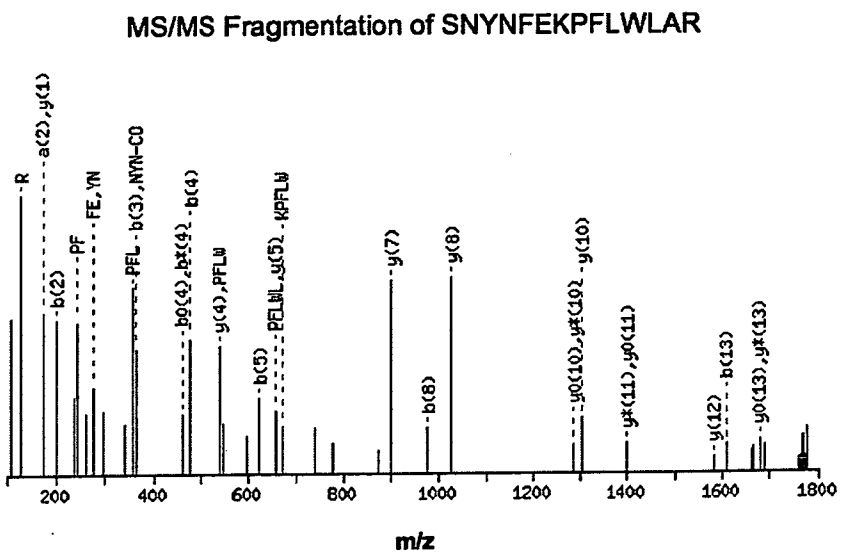

Fig. 3. Mass Spectrometry Analysis of Tryptic Digests of Proteins of Interest

Peptide mass fingerprinting and MS/MS analysis were performed using MALDI-TOF/TOF-MS. Ion peak spectra matched the five peptide sequences of the tryptic digests from spot number 25 in CM-treated HUVECs was detected (A) and MS/MS spectra of the precursor ion at m/z=1784.904 were shown (B).

Table 1. Identified Proteins of HUVECs Markedly Changed in the Spot Signals by Treatment with CM

Definition	Official symbol[a]	Spot number[b]	GI number	Fold change	pI	Mw[c]	Coverage (%)	Classification
Annexin A2, isoform 2	ANXA2	16	18645167	0.57	7.57	38784	45	Signal transduction
ARP1 actin-related protein 1 homolog A, centractin alpha	ACTR1A	10	5031569	0.64	6.19	42703	45	Cytoskeletal regulation
ATPase, H^+ transporting, lysosomal 70 kD, V1 subunit A, isoform 1	ATP6V1A	2	15341906	0.66	5.35	68667	3	Channel
Chain B, a short peptide insertion crucial for angiostatic activity of human tryptophanyl-tRNA synthetase	WARS2	7	42543731	0.49	6.41	44996	27	Protein synthesis
Chain B, human glutathione *S*-transferase P1-1 Y49f mutant	GSTP1	29	4699784	0.42	5.43	23577	30	Metabolism
Chain B, human heart L-lactate dehydrogenase H chain	LDHB	17	13786848	0.53	5.72	36774	29	Glycolytic enzyme
Chain H, Cys302ser mutant of human mitochondrial aldehyde dehydrogenase complexed with Nad^+ and Mg^{2+}	ALDH2	8	33357604	1.50	5.69	54859	44	Metabolism
Chaperonin containing TCP1, subunit 2	CCT2	6	5453603	0.64	6.01	57800	42	Chaperone
Chloride intracellular channel 4	CLIC4	20	7330335	0.54	5.45	28986	47	Channel
ENO1 protein (enolase 1, alpha)	ENO1	9	29792061	0.48	7.01	47487	24	Glycolytic enzyme
Eukaryotic translation initiation factor 3, subunit 3 gamma, 40 kDa	EIF3S3	13	4503515	0.55	6.09	40079	50	Protein synthesis
Glutathione-*S*-transferase omega 1	GSTO1	21	4758484	0.42	6.23	27838	17	Metabolism
Glyceraldehyde-3-phosphate dehydrogenase (GAPDH)	GAPDH	14	32891805	0.62	8.57	36204	23	Glycolytic enzyme
KIAA0098 (chaperonin containing TCP1, subunit 5 [epsilon])	CCT5	4	58257644	0.67	5.45	60664	39	Chaperone
KIAA0158 (septin 2)	SEPT2	11	40788885	0.65	6.05	42352	45	Unknown
Lamin A/C isoform 3	LMNA	1	27436948	0.63	8.55	70908	18	Structural protein
Peroxiredoxin 6	PRDX6	27	4758638	0.54	6	25135	26	Antioxidant enzyme
Phosphoglycerate mutase 1	PGAM1	22	38566176	0.46	6.67	28918	52	Glycolytic enzyme
Porin 31HM (voltage-dependent aninon channel 1)	VDAC1	18	238427	1.64	8.63	30739	32	Channel
Proteasome (prosome, macropain) 26S subunit, non-ATPase, 13	PSMD13	12	30583453	0.65	5.53	43181	44	Protein degradation
Proteasome alpha 6	PSMA6	24	23110944	0.60	6.34	27846	25	Protein degradation
Proteasome subunit HSPC	PSMA7	23	4092058	0.65	8.6	28060	45	Protein degradation
RAN protein (member RAS oncogene family)	RAN	25	32425497	0.60	7.16	25381	22	Signal transduction
Similar to triosephosphate isomerase 1 (LOC729708)		28	16877874	0.45	5.25	19038	33	Glycolytic enzyme
T-plastin polypeptide (plastin 3 [T form])	PLS3	3	190028	0.66	5.73	64289	4	Cytoskeletal regulation
TXNRD1 (thioredoxin reductase 1)	TXNRD1	5	49168498	0.56	6.07	55294	53	Antioxidant enzyme
Ubiquitin carboxyl-terminal esterase L1	UCHL1	26	21361091	0.36	5.33	25156	29	Protein degradation
Unknown		15	41472053	0.58	8.54	33672	29	Unknown
YWHAZ protein (tyrosine 3-monooxygenase/tryptophan 5-monooxygenase activation protein, zeta polypeptide)	YWHAZ	19	49119653	0.47	4.72	30103	31	Signal transduction

a) From NCBI Entrez Gene. *b*) Numbers corresponding to those in Fig. 2. *c*) Molecular weight of protein.

Among 3606 protein spots detected on the 2-D gel, 232 spots were found to be differentially expressed between treated and untreated samples by statistical analysis of protein spot signals using the Decyder program. Surprisingly, most differentially expressed proteins in HT1080-CM-treated ECs were downregulated (204 proteins, 88%) rather than upregulated (28 proteins, 12%) in our proteomics. Among these, 29 protein species were successfully identified by MALDI-TOF/TOF-MS analysis (Table 1, Fig. 3), and these could be functionally classified into glycolytic enzymes, protein degradation-related proteins, proteins involved in signal transduction, and others (Table 1). Two identified proteins, ALDH2 (related to metabolism) and voltage-dependent anion channel 1 (VDAC1), were upregulated by HT1080-CM treatment (Fig. 4), but all the others were downregulated. The representatives of downregulated proteins and their functional classification were: (1) enolase 1 (ENO1, Fig. 4), LDHB, GAPDH, PGAM1, and similar to triosephosphate isomerase (glycolytic enzymes); (2) PSMD13, PSMA6, PSMA7, and UCHL1 (protein degradation-related proteins); (3) annexin A2 (ANXA2), RAN (Fig. 4), and YWHAZ (signal transduction-related proteins); and (4) PRDX6 and

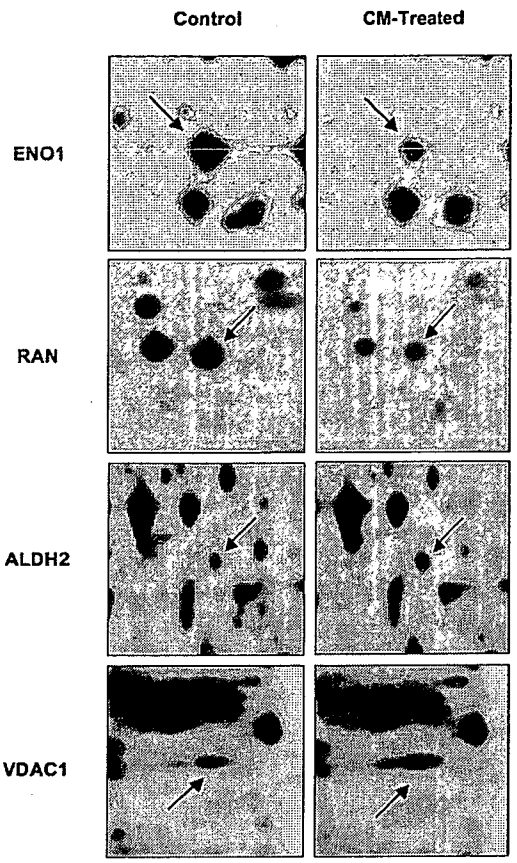

Fig. 4. Representative Proteins Markedly Changed in Expression by Treatment with HT1080-CM

Proteomic analysis was performed as described in the legend to as Fig. 2 and in Materials and Methods. The expression of ENO1 and RAN was decreased in CM-treated HUVECs. Arrows indicate the protein spots of ENO1 and RAN.

TXNRD1 (antioxidant enzymes).

Differentially Expressed Proteins in Response to VEGF Stimulation We additionally analyzed the protein expression changes in HUVECs in response to VEGF stimulation using 2D-DIGE (Fig. 5). Among 3,924 protein spots detected, 159 proteins were found to be differentially expressed between treated and untreated samples by statistical analysis, and 94 protein spots (59%) were upregulated and 65 (41%) were downregulated. Among these 159 protein spots, 35 species were identified by MALDI-TOF/TOF-MS (Table 2) and these were functionally classified into proteins related to cytoskeletal regulation, protein synthesis, RNA processing, and signal transduction. The differentially expressed proteins and their functional classification represented were: (1) CALD1, GSN, T-plastin (PSL3), and LASP1 (all upregulated, cytoskeleton-regulating proteins); (2) EEF1B2, EEF1D, EEF2, and EEF1A1L14 (all upregulated, protein synthesis-related proteins); (3) ANXA1, ANXA2 and ANXA5 (all upregulated), and RAN (downregulated) (signal transduction-related proteins); (4) HNRPC, HNRPA1, RBM8A, and SFRS3 (all downregulated, RNA processing); and (5) SDHA, UQCRC1, COX4NB, and ATP5H (all downregulated, mitochondrial electron transport system). In the identified proteins, some of which are known to be associated with angiogenesis induced by VEGF (HSP90, HSP70, EEF, ENO1, *etc.*),[6] and others may be novel proteins associated with VEGF-induced angiogenesis (LASP1, RAN, UQCRC1, *etc.*).

Comparison of CM-Induced and VEGF-Induced Angiogenic Response in HUVECs Based on the data as described above, the expression profiles of identified proteins were compared between CM-induced and VEGF-induced response in HUVECs. By statistical analysis of protein spot signals using the Decyder software program, protein expression was predominantly suppressed (88%) rather than induced (12%) by HT1080-CM stimulation, whereas the expression was predominantly induced (59%) rather than suppressed (41%) by VEGF stimulation. As shown in Fig. 6, the identified protein species in the CM-induced angiogenic response were markedly different from those in the VEGF-induced response. Among the total 60 protein species identified, only four species were either up- or downregulated in both CM and VEGF stimulation (Fig. 6A). We did not find the proteins upregulated by both CM and VEGF stimulation (Fig. 6B), but RAN was found to be downregulated by both stimulations (Fig. 6C). There was no protein upregulated by CM and downregulated by VEGF (Fig. 6D), while three proteins (ANXA2, ENO1 (Fig. 4), and PSL3) were found to be downregulated by CM but upregulated by VEGF (Fig. 6E).

DISCUSSION

Angiogenesis is a critical event for tumor growth and hematogenous metastasis,[1] and VEGF has been well characterized as a regulator of angiogenesis.[4] However, the VEGF stimulation of ECs as an angiogenic model is not thought to reflect the condition of actual tumor angiogenesis. The CM stimulation of ECs is probably a better cellular model for tumor angiogenesis, because cancer cells produce several proangiogenic factors and inhibitors.[2] The CM prepared from HT1080 fibrosarcoma cells enhanced the cell proliferation and tube formation mimicking the tumor angiogenesis processes.

To our knowledge, this proteomic study is the first demonstration that (1) HT1080-CM predominantly induced the downregulation rather than the upregulation of protein expression in HUVECs; (2) the identified proteins of ECs stimulated with CM were considerably different from those stimulated with VEGF; (3) two proteins, ALDH2 and VDAC1, were upregulated by CM in their expression; (4) three proteins, ANXA2, ENO1, and PLS3, were downregulated by CM, but upregulated by VEGF in their expression; and (5) no proteins were found to be upregulated by both CM and VEGF stimulation, but the downregulation of RAN by both was detected.

ALDH2 is a member of the aldehyde dehydrogenase family and is involved in the oxidative pathway of alcohol metabolism. The relationship between alcohol metabolism and cancer progression has previously been well studied, and the acetaldehyde plays a critical role in field cancerization.[11] Recently, Chen *et al.* have reported that an inhibitor of aldehyde dehydrogenase, disulfiram (DSF), induced apoptosis in breast cancer cells and suppressed tumor growth.[12] In this study, ALDH2 expression was found to be upregulated by treatment with HT1080-CM but not with VEGF. Inhibition of ALDH2 enzyme activity by certain therapeutic agents may be useful for the suppression of cancer-mediated angiogenesis.

Table 2. Identified Proteins of HUVECs Markedly Changed in the Spot Signals by Treatment with VEGF

Definition	Official symbol[a]	Spot number[b]	GI number	Fold change	pI	Mw[c]	Coverage (%)	Classification
ACTB protein (actin, beta)	ACTB	15	15277503	1.59	5.55	40542	41	Cytoskeletal regulation
Aldehyde dehydrogenase 1	ALDH1A1	11	2183299	0.65	6.3	55438	19	Metabolism
Annexin 5	ANXA5	22	4502107	1.78	4.94	35972	23	Signal transduction
Annexin A2, isoform 2	ANXA2	24	16306978	1.51	7.57	38826	23	Signal transduction
Annexin I	ANXA1	19	4502101	1.53	6.57	38922	36	Signal transduction
Caldesmon 1 isoform 2	CALD1	4	4826657	1.56	6.18	62683	38	Cytoskeletal regulation
Catalase	CAT	10	4557014	0.61	6.9	59951	17	Antioxidant enzyme
Chain A, triosephosphate isomerase (Tim) (EC 5.3.1.1) complexed with 2-phosphoglycolic acid		27	999892	1.51	6.51	26812	45	Glycolytic enzyme
EH-domain containing protein 2	EHD2	8	57015322	1.67	5.95	61184	18	Unknown
Enolase 1	ENO1	13	4503571	2	7.01	47487	34	Glycolytic enzyme
Eukaryotic translation elongation factor 1 beta 2	EEF1B2	21	4503477	1.69	4.5	14922	27	Protein synthesis
Eukaryotic translation elongation factor 1 delta isoform 2 (guanine nucleotide exchange protein)	EEF1D	18	25453472	1.58	4.9	31219	26	Protein synthesis
Eukaryotic translation elongation factor 2	EEF2	1	4503483	1.53	6.41	96246	31	Protein synthesis
Gelsolin isoform b	GSN	3	38044288	1.86	5.58	80876	19	Cytoskeletal regulation
Heat shock 70 kDa protein 8 isoform 1	HSPA8	5	5729877	1.71	5.37	70186	42	Chaperone
Heat shock 90 kDa protein 1, beta	HSP90AB1	2	20149594	1.52	4.97	83554	44	Chaperone
Heterogeneous nuclear ribonucleoprotein A1 isoform a	HNRPA1	22	4504445	0.66	9.27	34291	35	RNA processing
Heterogeneous nuclear ribonucleoprotein C isoform b	HNRPC	16	4758544	0.63	5.1	32005	27	RNA processing
LIM and SH3 protein 1	LASP1	20	5453710	1.56	6.61	30104	28	Cytoskeletal reguration
MDS014 (RNA binding motif protein 8A)	RBM8A	34	10197630	0.57	6.46	18264	31	RNA processing
My032 protein (ATP synthase, H^+ transporting, mitochondrial F0 complex, subunit d)	ATP5H	30	12002006	0.65	6.6	15821	70	Mitochondrial electron transport chain
Neighbor of COX4	COX4NB	29	5174615	0.52	5.92	24222	31	Mitochondrial electron transport chain
Peroxiredoxin 1	PRDX1	31	4505591	1.64	8.27	22328	42	Antioxidant enzyme
RAN protein (member RAS oncogene family)	RAN	28	32425497	0.61	7.16	25381	30	Signal transduction
Similar to Homo sapiens mRNA for KIAA0120 gene with GenBank accession number D21261.1		32	9956026	1.6	8.41	24438	84	Unknown
Splicing factor, arginine/serine-rich 3	SFRS3	35	4506901	0.64	11.64	19318	24	RNA processing
Succinate dehydrogenase complex, subunit A, flavoprotein precursor	SDHA	7	4759080	0.6	7.06	73687	30	Mitochondrial electron transport chain
TALDO1 protein (transaldolase 1)	TALDO1	17	17511894	1.57	6.36	37690	27	Pentose phosphate pathway
TKT protein (discoidin domain receptor family, member 2)	DDR2	6	31417921	1.61	8.02	50543	35	Pentose phosphate pathway
T-plastin polypeptide (plastin 3 [T form])	PSL3	9	190028	1.93	5.73	64289	46	Cytoskeletal regulation
TPM4-ALK fusion oncoprotein type 2		25	10441386	1.93	4.77	27571	23	Cytoskeletal regulation
TPMsk3 (tropomyosin 3)	TPM3	26	19072649	1.84	4.72	28908	23	Cytoskeletal regulation
Transgelin 2	TAGLN2	33	4507357	1.84	8.41	22377	84	Unknown
Translation elongation factor 1 alpha 1-like 14	EEF1A1L14	12	15277711	1.56	9.1	50457	23	Protein synthesis
Ubiquinol-cytochrome c reductase core protein I	UQCRC1	14	46593007	0.58	5.94	53281	8	Mitochondrial electron transport chain

a) From NCBI Entrez Gene. *b*) Numbers corresponding to those in Fig. 5. *c*) Molecular weight of protein.

VDAC1, an outer membrane protein of mitochondria, is a small and abundant pore-forming protein thought to form the major pathway for the movement of adenine nucleotides through the mitochondrial membrane. This protein is also known as a receptor for plasminogen kringle 5, which induces apoptosis of endothelial cells and regulates angiogenesis.[13] The direct relationship between VDAC1 and angiogenesis, however, is still unclear. Since HT1080-CM-stimulated endothelial cells highly express VDAC1 as well as malignant cells,[14] it might be a candidate as an effective target for cancer therapy.

ANXA2 is a member of the calcium-dependent phospholipid-binding protein family and known to play a role in the regulation of cellular growth and signal transduction. The expression of ANXA2 is known to be upregulated in various types of cancers such as pancreas, breast, and brain[15] and in tumor vasculature,[16] whereas its expression was downregulated in prostate cancer.[17] Since our results showed that ANXA2 expression was downregulated by HT1080-CM but upregulated by VEGF, HT1080-CM treatment may cause a response similar to prostate cancer. ANXA2 is also a cell surface receptor for angiostatin, which is a potent endoge-

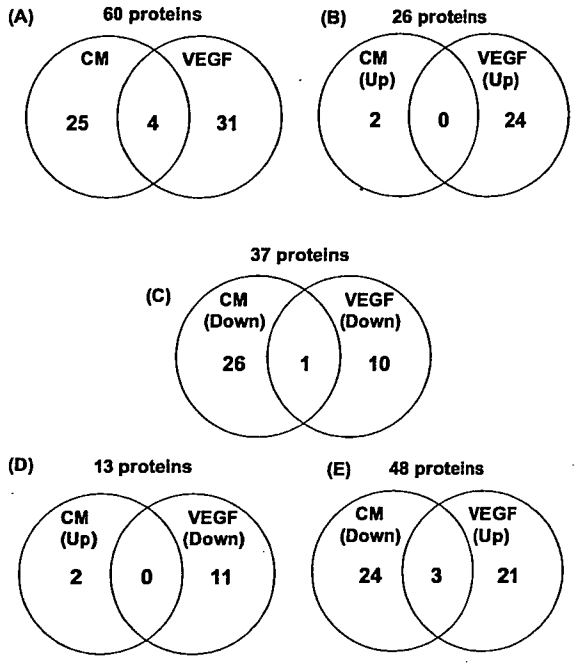

Fig. 6. Comparative Analysis of Protein Molecules in CM-Induced and VEGF-Induced Angiogenic Response

(A) Total 60 differentially expressed proteins; (B) proteins upregulated by both CM and VEGF stimulation; (C) those downregulated by both; (D) those upregulated by CM and downregulated by VEGF; (E) proteins downregulated by CM but upregulated by VEGF treatment. Numbers of the overlapping circles in the Venn diagrams shows the number of protein species differentially expressed in both types of stimulation.

nous angiogenesis inhibitor.[18] It was reported that angiostatin can suppress tumor growth and metastasis in various cancers.[19,20] It is possible that the downregulation of ANXA2 expression by HT1080-CM promotes CM-induced angiogenesis through the suppression of the effect of angiostatin.

ENO1 is a glycolytic enzyme and has been found to bind to an element in the c-myc promoter. Recently, it has been reported that ENO1 suppresses prostate cancer cell growth and induces neuroblastoma cell death.[21,22] Hence the downregulation of ENO1 induced by HT1080-CM might promote endothelial cell growth.

PLS3 is a member of an important actin-filament cross-linking protein family and controls cell motility by the maintenance of the actin cytoskeleton. This protein enhances actin base cell movement mediated by the Wiskott/Aldrich-symdrom protein (WASP).[23] Since WASP plays an important role in endothelial cell movement,[24] PLS3 might be associated with cellular motility during the HT1080-CM-regulated angiogenic response.

RAN is a small GTP-binding and Ras-related nuclear protein with an important role in the transport of RNA and proteins through the nuclear pore complex. This protein positively regulates the nuclear localization of PTEN, one of the important tumor-suppressor gene products, and nuclear PTEN is known to enhance apoptosis.[25] PTEN negatively controls the Akt signal-transduction pathway and is also closely associated with angiogenesis.[26] Downregulation of RAN by CM and VEGF might suppress the nuclear translocation of PTEN and promote angiogenesis.

In addition to these proteins, we identified some functional protein molecules that may be involved in CM-induced angiogenic response, such as glycolytic enzymes, protein degradation-related proteins, and antioxidant enzymes. Among them, UCHL1, which plays a role in proteasomal protein degradation, was reported to be reduced in metastatic melanoma and showed inhibitory effects on the metastasis of melanoma.[27]

As mentioned above, the differential expression of ALDH2, VDAC1, ANXA2, ENO1, PLS3, RAN, *etc.* in HT1080-CM-induced angiogenesis seems to be associated with cancer cell-mediated angiogenesis. Thus our data provide new information regarding the regulation of protein expression associated with tumor-induced angiogenesis and will be helpful in understanding the molecular mechanisms of tumor angiogenesis.

Acknowledgments This research was supported by Center of Exellence (COE) program in the 21st Century and Cooperation of Innovative Technology and Advanced Research in Evolutional Area (CITY AREA) to N. Oku and N. Ohashi from the Ministry of Education, Culture, Sports, Science and Technology of Japan.

REFERENCES

1) Carmeliet P., Jain R. K., *Nature* (London), **407**, 249—257 (2000).
2) Bergers G., Benjamin L. E., *Nat. Rev. Cancer*, **3**, 401—410 (2003).
3) Neri D., Bicknell R., *Nat. Rev. Cancer*, **5**, 436—446 (2005).
4) Cross M. J., Dixelius J., Matsumoto T., Claesson-Welsh L., *Trends Biochem. Sci.*, **28**, 488—494 (2003).
5) Abe M., Sato Y., *Angiogenesis*, **4**, 289—298 (2001).
6) Pawlowska Z., Baranska P., Jerczynska H., Koziolkiewicz W., Cierniewski C. S., *Proteomics*, **5**, 1217—1227 (2005).
7) Griffin T. J., Gygi S. P., Ideker T., Rist B., Eng J., Hood L., Aebersold R., *Mol. Cell. Proteomics*, **1**, 323—333 (2002).
8) Petricoin E. F., Zoon K. C., Kohn E. C., Barrett J. C., Liotta L. A., *Nat. Rev. Drug Discovery*, **1**, 683—695 (2002).
9) Unlu M., Morgan M. E., Minden J. S., *Electrophoresis*, **18**, 2071—2077 (1997).
10) Ibuki Y., Naitou H., Ohashi N., Goto R., *Photochem. Photobiol.*, **81**, 823—829 (2005).
11) Muto M., Nakane M., Hitomi Y., Yoshida S., Sasaki S., Ohtsu A., Yoshida S., Ebihara S., Esumi H., *Carcinogenesis*, **23**, 1759—1765 (2002).
12) Chen D., Cui Q. C., Yang H., Dou Q. P., *Cancer Res.*, **66**, 10425—10433 (2006).
13) Gonzalez-Gronow M., Kalfa T., Johnson C. E., Gawdi G., Pizzo S. V., *J. Biol. Chem.*, **278**, 27312—27318 (2003).
14) Liu S., Ishikawa H., Tsuyama N., Li F. J., Abroun S., Otsuyama K. I., Zheng X., Ma Z., Maki Y., Iqbal M. S., Obata M., Kawano M. M., *Oncogene*, **25**, 419—429 (2006).
15) Emoto K., Sawada H., Yamada Y., Fujimoto H., Takahama Y., Ueno M., Takayama T., Uchida H., Kamada K., Naito A., Hirao S., Nakajima Y., *Anticancer Res.*, **21**, 1339—1345 (2001).
16) Oh P., Li Y., Yu J., Durr E., Krasinska K. M., Carver L. A., Testa J. E., Schnitzer J. E., *Nature* (London), **429**, 629—635 (2004).
17) Chetcuti A., Margan S. H., Russell P., Mann S., Millar D. S., Clark S. J., Rogers J., Handelsman D. J., Dong Q., *Cancer Res.*, **61**, 6331—6334 (2001).
18) Syed S. P., Martin A. M., Haupt H. M., Arenas-Elliot C. P., Brooks J. J., *Hum. Pathol.*, **38**, 508—513 (2007).
19) Sharma M. R., Rothman V., Tuszynski G. P., Sharma M. C., *Exp. Mol. Pathol.*, **81**, 136—145 (2006).
20) Wahl M. L., Kenan D. J., Gonzalez-Gronow M., Pizzo S. V., *J. Cell. Biochem.*, **96**, 242—261 (2005).
21) Ejeskar K., Krona C., Caren H., Zaibak F., Li L., Martinsson T., Ioannou P. A., *BMC Cancer*, **5**, 161 (2005).
22) Ghosh A. K., Steele R., Ray R. B., *J. Biol. Chem.*, **280**, 14325—14330 (2005).
23) Giganti A., Plastino J., Janji B., Van Troys M., Lentz D., Ampe C., Sykes C., Friederich E., *J. Cell Sci.*, **118**, 1255—1265 (2005).

Available online at www.sciencedirect.com
ScienceDirect
Journal of Controlled Release 126 (2008) 162–165
journal of controlled release
www.elsevier.com/locate/jconrel

Rapid communication

The contribution of phagocytic activity of liver macrophages to the accelerated blood clearance (ABC) phenomenon of PEGylated liposomes in rats

Tatsuhiro Ishida, Syuntaro Kashima, Hiroshi Kiwada *

Department of Pharmacokinetics and Biopharmaceutics, Subdivision of Biopharmaceutical Sciences, Institute of Health Bioscience, The University of Tokushima, 1-78-1, Sho-machi, Tokushima 770-8505, Japan

Received 9 September 2007; accepted 16 November 2007
Available online 24 November 2007

Abstract

We earlier reported that PEGylated liposomes lose their long-circulating property when they are administered twice in the same animal within certain intervals. We recently proposed that anti-PEG IgM elicited by the first dose PEGylated liposomes selectively binds to the surface of a second dose, subsequently leading to substantial complement activation and complement-receptor mediated uptake of the second dose by hepatic Kupffer cells. In this study we found, by using a single-pass liver perfusion technique, that the first dose does not increase the intrinsic phagocytic activity of the Kupffer cells. It was also found that only serum obtained from rats that had received a first dose is able to enhance the hepatic uptake of test dose. The conditioned-serum-dependent hepatic uptake was completely abolished by pre-treatment of the serum at 56 °C for 30 min, which inhibits the complement activity. Conclusively, our results strongly support our earlier proposal that complement activation caused by anti-PEG IgM elicited by the first dose is a major cause of the initiation of the accelerated blood clearance of a subsequent dose PEGylated liposome in the ABC phenomenon.

Keywords: Accelerated blood clearance (ABC) phenomenon; PEGylated liposome, Polyethylene glycol (PEG); Liver perfusion; Complement system

1. Introduction

PEGylated liposomes, which have long-circulating properties, have been amply used as a drug carrier to improve the circulation lifetime of entrapped therapeutic agents [1]. It is believed that the PEG on the surface of liposomes, providing a steric barrier against the attachment of plasma proteins such as opsonins and recognition by the cells of the mononuclear phagocyte system, in turn, results in a decrease in the rate of clearance of the liposomes from blood circulation [2]. However, we and other researchers have observed that the first dose PEGylated liposomes cause a second dose, injected several days later, to lose its long-circulating properties and to accumulate extensively in the liver in mice, rats and rhesus monkeys (referred to as the "accelerated blood clearance (ABC) phenomenon") [3–6]. Based on our recent studies [7–9], we proposed the following tentative mechanism for the induction of the ABC phenomenon: anti-PEG IgM, produced by the spleen in response to the first dose, selectively binds to the PEG chains on a second dose administered several days later, and subsequently activates the complement system, one of the major opsonins [10–12], and enhances uptake of the second dose by the Kupffer cells [3,5,13].

Two phases can be distinguished in the ABC phenomenon [5,8]: the induction phase, following the first injection, during which the immune system is primed [reflected in the production of anti-PEG IgM], and the effectuation phase, following the second injection, during which the PEGylated liposomes are

Abbreviations: ABC, accelerated blood clearance; CHOL, cholesterol; HEPC, hydrogenated egg phosphatidylcholine; $mPEG_{2000}$-DSPE, 1,2-distearoyl-*sn*-glycero-3-phosphoethanolamine-*n*-[methoxy(polyethylene glycol)-2000]; PEG, polyethylene glycol.

* Corresponding author. Tel.: +81 88 633 7259; fax: +81 88 633 9506.
E-mail address: hkiwada@ph.tokushima-u.ac.jp (H. Kiwada).

0168-3659/$ - see front matter © 2007 Elsevier B.V. All rights reserved.
doi:10.1016/j.jconrel.2007.11.009

rapidly cleared from the blood circulation [reflected in enhanced uptake by Kupffer cells]. Earlier studies indicated that Kupffer cells are at least partly responsible for the effectuation phase [3,5,9]. Thus, it is tempting to assume that liver macrophages acquire the ability to recognize and avidly take up PEGylated liposomes as the ABC phenomenon developed.

Therefore, in this study we investigated the issue of whether the injection of PEGylated liposomes increases the intrinsic, opsonin-independent, phagocytic activity of the Kupffer cells. Furthermore, we addressed the issue of whether the complement activation synergistically enhances the uptake of the second dose, resulting in a further increase in Kupffer cell-mediated liver uptake. To that end we employed a single-pass liver perfusion technique [14–16], because this method allows us to evaluate the issues under conditions at which the influence of serum is included or excluded.

2. Materials and methods

2.1. Materials and animal

Hydrogenated egg phosphatidylcholine (HEPC) and 1,2-distearoyl-*sn*-glycero-3-phosphoethanolamine-*n*-[methoxy(polyethylene glycol)-2000] ($mPEG_{2000}$-DSPE) were generously donated by Nippon Oil and Fat (Tokyo, Japan). Cholesterol (CHOL) was of analytical grade (Wako Pure Chemical, Osaka, Japan). All lipids were used without further purification. ^{3}H-Cholesterylhexadecyl ether (^{3}H-CHE) was purchased from PerkinElmer Japan (Yokohama, Japan). All other reagents were of analytical grade.

Male Wistar rats (250–300g) were purchased from Japan SLC (Shizuoka, Japan). All animal experiments were evaluated and approved by the Animal and Ethics Review Committee of the University of Tokushima.

2.2. Preparation of liposomes

PEGylated liposomes, composed of HEPC:CHOL:$mPEG_{2000}$-DSPE (1.85:1.0:0.15 molar ratio), were prepared as previously described [6]. The mean diameter of the prepared liposomes was determined by using a NICOMP 370 HPL submicron particle analyzer (Particle Sizing System, CA, USA). The concentration of phospholipid was determined by colorimetric assay [17].

2.3. In situ a single-pass liver perfusion study

Rats had received an intravenous injection of PEGylated liposome (0.001 μmol/kg) or HEPES-buffered saline (pH 7.4) 5 days before were being subjected to the liver perfusion study described in the following. Perfused liver was prepared according to the method reported previously [14–16]. After a stabilization period of 10 min perfusion with Krebs–Ringer solution (pH 7.4) at a rate of 20 ml/min, radiolabeled test-dose PEGylated liposomes (4 mM in 7 ml of HEPES-buffered saline or serum) were infused via the portal vein at a constant rate (1 ml/min) for 7 min, following incubation with HEPES-buffered saline or serum at 37 °C for 15 min. After a 3-min wash with liposome-free perfusate, the liver was removed and weighed, and the radioactivity in whole liver was measured according to the method reported previously [18]. The uptake of liposomes was expressed as extraction (the percentage uptake of liposomes by the liver). Satisfactory liver viability was assessed on the basis of a bile flow rate >1 μl/min/g liver. Four to five rats were used in each group.

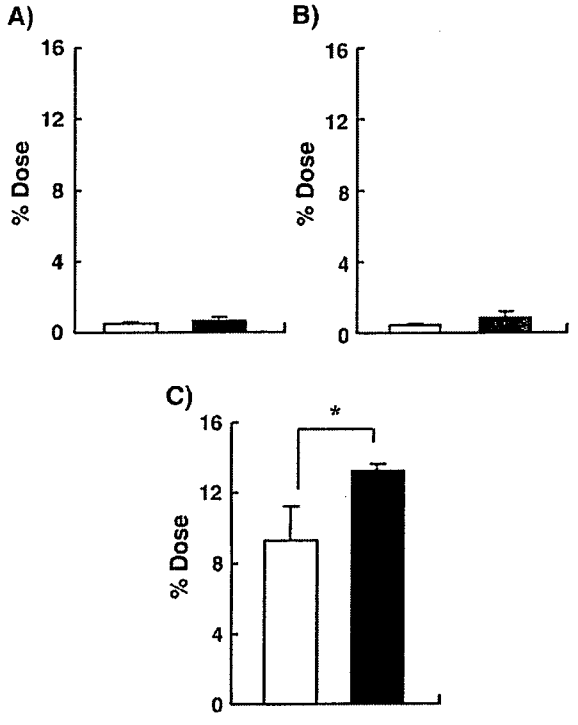

Fig. 1. Hepatic uptake of radiolabeled test-dose PEGylated liposomes in a single-pass liver perfusion. PEGylated liposomes (0.001 μmol phospholipids/kg) or HEPES-buffered saline was intravenously injected into rats. Five days later, a single-pass liver perfusion was carried out with pre-treated rats, using differently prepared radiolabeled test dose PEGylated liposomes. Open columns represent livers of rats (n=4–5) that had received HEPES-buffered saline. Filled columns represent livers of rats (n=4–5) that were pre-dosed with PEGylated liposomes. (A) test-dose liposomes were incubated with HEPES-buffered saline. (B) test-dose liposomes were incubated with serum from rats that had only received HEPES-buffered saline. (C) test-dose liposomes were incubated with serum from rats pre-dosed with PEGylated liposome. Each value represents the mean±S.D. of 4 or 5 separate experiments. * $p<0.05$.

2.4. Statistics

All values are expressed as the mean±S.D. Statistical analysis was performed with a two-tailed unpaired t test using GraphPad InStat software (GraphPad Software, CA, USA). The level of significance was set at $p<0.05$.

3. Results and discussion

3.1. Effect of pre-dose of PEGylated liposomes on the intrinsic phagocytic activity of liver macrophages towards test-dose PEGylated liposomes

To study the effect of pre-dose PEGylated liposomes on the intrinsic phagocytic activity of liver macrophages, we perfused rat livers with a pre-dose PEGylated liposomes (0.001μmol